

Ecological landscapes guide the assembly of optimal microbial communities

Ashish B. George^{1,2,3,*} and Kirill S. Korolev^{1,2,4,*}

¹ *Department of Physics, Boston University, Boston, MA 02215, USA*

² *Biological Design Center, Boston University, Boston, MA 02215, USA*

³ *Carl R. Woese Institute for Genomic Biology and Department of Plant Biology, University of Illinois at Urbana-Champaign, Urbana, IL 61801, USA*

⁴ *Graduate Program in Bioinformatics, Boston University, Boston, MA 02215, USA*

* Correspondence to: ashish.b.george@gmail.com, korolev@bu.edu

December 17, 2021

Abstract

Assembling optimal microbial communities is key for various applications in biofuel production, agriculture, and human health. Finding the optimal community is challenging because the number of possible communities grows exponentially with the number of species, and so an exhaustive search cannot be performed even for a dozen species. A heuristic search that improves community function by adding or removing one species at a time is more practical, but it is unknown whether this strategy can discover an optimal or nearly optimal community. Using consumer-resource models with and without cross-feeding, we investigate how the efficacy of search depends on the distribution of resources, niche overlap, cross-feeding, and other aspects of community ecology. We show that search efficacy is determined by the ruggedness of the appropriately-defined ecological landscape. We identify specific ruggedness measures that are both predictive of search performance and robust to noise and low sampling density. The feasibility of our approach is demonstrated using experimental data from a soil microbial community. Overall, our results establish the conditions necessary for the success of the heuristic search and provide concrete design principles for building high-performing microbial consortia.

Keywords: community assembly, microbiome, consumer-resource model, community design, cross-feeding

Introduction

Life on earth is sustained by a myriad of biochemical transformations. From synthesis to decomposition, microbial communities perform the bulk of these transformations, including photosynthesis, nitrogen fixation, and the digestion of complex molecules [1–3]. This understanding has generated considerable interest in exploiting microbial capabilities for producing energy and food, degrading waste, and improving health [4–10].

The metabolic ingenuity of microbial communities can be harnessed by simply placing the right

combination of species in the right environment. Yet, the search for the appropriate species and environmental conditions is anything but simple. Ecological interactions are nonlinear and often unpredictable, so an exhaustive search across all relevant variables is the only sure way to build a community with the best performance. Such an exhaustive search is however infeasible because the number of possible combinations increases exponentially with the number of species and environmental factors; just 16 species leads to over 65,000 combinations. Even with expert knowledge, computer simulations, and liquid-handling robots, exhaustive testing remains infeasible for any complex microbial community [11–19].

This challenge is not unique to ecology. In fact, most optimization problems cannot be solved directly, and one has to resort to heuristic search strategies [20, 21]. For microbial communities, a simple heuristic search (a greedy gradient-ascent) proceeds via a series of steps. At each step, a set of new communities is created by adding or removing one or a few species from the current microbial community. The community with the best performance is then chosen for the next step. Although easy to implement, the search can get stuck at a local optimum and achieve only a small fraction of the best possible performance. It is therefore essential to identify when such heuristic search is likely to succeed.

Here, we study the success of the heuristic search by simulating a range of realistic and widely-used *consumer-resource* models of microbial communities, which have reproduced many features of natural and experimental communities [22–24]. In the simulated communities, microbes compete for externally supplied resources and potentially produce other metabolites that can be exchanged among the community members. Our simulations allowed us to vary the complexity of the microbial ecosystem and explore its effects on the efficacy of the search. We identified specific ecological properties, such as the average niche overlap, to be highly predictive of the search success.

To integrate our findings into a coherent framework and understand when search fails, we define and analyze community function landscapes utilizing an analogy to the fitness landscapes from population genetics [25]. The community function of interest is analogous to fitness, and the composition of the community is analogous to the genome. The heuristic search then corresponds to an uphill walk on this multi-dimensional landscape. Similar to previous studies in evolution, we found that search success depends on the *ruggedness* of the ecological landscape. Multiple definitions of ruggedness exist, and we identified those that are more predictive across diverse ecological scenarios and can be reliably estimated from limited, noisy experimental data. The intuition gained from our numerical studies applied well to real experimental data on an ecological landscape for six soil microbes from Ref. [26].

Overall, our work identifies the connections between ecological properties, community structure, and optimization. This knowledge makes it possible to predict whether heuristic search is feasible and provides concrete strategies to increase the chance of success by adjusting the environment or the pool of candidate species. Furthermore, we anticipate that community landscapes can provide a unifying framework to compare microbial consortia and their assembly across diverse ecological settings.

Outcome of dynamics	Models and experiments
Single steady state	Consumer-resource models with substitutable resources: [27–31]. Consumer-resource models with cross-feeding: [32, 33]. Many Lotka-Volterra models including those with random interactions with low to moderate variance: [34–39] Compatible empirical observations: [40–42].
Typically a single steady state	Consumer resource models with non-substitutable resources or species consuming resources diauxically: [43, 44]. Compatible empirical observations: [45, 46].
Multiple steady states	Lotka-Volterra models with random interactions with large variance: [34, 35]. Compatible empirical observations: [47, 48].
Complex dynamics and chaos	Stochastic neutral models: [49, 50]. Consumer resource models with highly nonlinear uptake of non-substitutable resources: [28, 31, 51]. Lotka-Volterra models with antisymmetric interactions or random interactions with large variance: [34, 52]. Compatible empirical observations: [53].

Table 1: Microbial communities often converge to a unique steady state, but more complex dynamics are possible. Macroscopic organisms are discussed in Ref. [54].

Model

We simulated microbial communities using consumer-resource models with and without cross-feeding [27, 32]. Compared to the commonly-used Lotka-Volterra models, our approach is more realistic and makes a closer connection to the metabolic interactions that underpin many optimization problems in biotechnology [55–59]. Furthermore, it is much easier to make educated guesses about the production and consumption of resources than interaction coefficients. One disadvantage of our approach is that other interactions, such as due to various antimicrobials, are excluded. Although such interactions play a prominent role in natural communities, they are often removed or otherwise controlled in engineered communities.

We assume that the growth of each microbe depends on its ability to consume various available resources and convert consumed resources into biomass. The resources could be externally supplied or excreted by the microbes themselves as metabolic byproducts [32, 60–63]. Both the species and the resources are diluted at a fixed rate to prevent the accumulation of nutrients and biomass, as in a chemostat. The mathematical details of the models are further explained in Methods. Numerical simulations were carried out using code based on the ‘Community Simulator’ package [64].

The ecological dynamics could, in principle, be time-dependent or sensitive to the species abundances at the beginning of the experiment. For consumer-resource models, however, the community always reaches a unique steady-state that depends only on the initial presence or absence of species. Recent studies show that time-dependence and multi-stability are more of an exception than the norm and most (especially engineered) communities exhibit the simple behavior of consumer-resource models (see Table 1 and Ref. [65–67]).

The search for the optimal community begins with a choice of the desired ecological function, denoted as \mathcal{F} ; this could be the production rate of a particular metabolite, the degradation rate of an undesirable compound, or even the diversity of the community. One also needs to choose the pool of S candidate species from which to assemble the microbial community. In total, there are 2^S possible communities, corresponding to distinct species combinations that can be labeled by $\vec{\sigma}$, a string of ones and zeros denoting the presence or absence of each species in the starting community (Fig. 1). The simplest search protocol starts with one of the 2^S possibilities, for e.g., the community with all species present. Then, every step of the search is a heuristic gradient-ascent, which considers the current community and the S neighboring communities obtained by changing each of the elements of $\vec{\sigma}$, i.e., adding or removing a species. These communities are simulated until they reach a steady state, and the community with the highest value of \mathcal{F} is taken to be the next current state. The process repeats until the community function cannot be improved any further by adding or removing a single species. We also explore several variations of this search protocol after obtaining the main results in the context of the search protocol just described.

Because consumer-resource models reach a unique steady state, all quantities that depend on species and resource concentrations are uniquely determined by the presence-absence of species at the beginning of the simulation. Thus, the community function is fully determined by $\vec{\sigma}$. The search for the optimal community then reduces to the maximization of \mathcal{F} over $\vec{\sigma}$, and $\mathcal{F}(\vec{\sigma})$ can be viewed as a multi-dimensional ecological or community function landscape. Mathematically, this landscape is related to the fitness landscapes studied in population genetics [25], with \mathcal{F} analogous to fitness and $\vec{\sigma}$ analogous to genotype. Below, we explore the structure of ecological landscapes under different ecological conditions and examine the influence of landscape structure on the success of

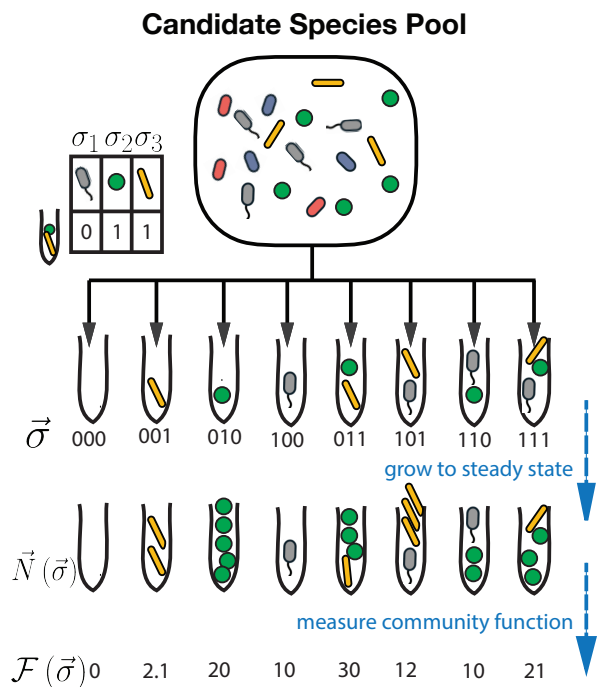


Figure 1: **An ecological landscape framework for community optimization.** We consider the problem of assembling an ecological community from a pool of S candidate species that is optimal at performing a desired function. The candidate species in the pool are indexed from 1 to S . A test community is seeded with a subset of the candidate species. The composition of the community is encoded in $\vec{\sigma}$ using 0 for absence and 1 for presence for each of the species. The test communities are allowed to grow until they reach a steady state. The species abundances in the steady-state community is $\vec{N}(\vec{\sigma})$, and the community function is $\mathcal{F}(\vec{\sigma})$.

the heuristic search.

Results

Niche overlap controls the complexity of ecological landscapes

The problem of finding optimal microbial communities brings a number of questions about the landscape structure and its influence on search success. Before we begin to explore these questions in detail, it is convenient to establish how one can control the difficulty of the search by varying a relevant ecological variable. Intuition suggests that communities with many inter-specific interactions should be more complex than communities where species are largely independent from each other. Therefore, we explored how the density of metabolic interactions influences community structure.

The density of interactions is controlled by the overlap in the resource utilization profiles of the species in the community. Simply put, the more species consume any given resource, the greater the number of interactions. In our model, these interactions are encoded in the consumption matrix; see Fig. 2A. We created these matrices by allowing each species to consume only a random subset

of M_{consumed} resources out of M_{total} resources supplied externally.

When $M_{\text{consumed}} \approx M_{\text{total}}$, the species are generalists; several species are consuming each of the resources, and the niche overlap is high (Fig. 2B). In the opposite limit ($M_{\text{consumed}} \ll M_{\text{total}}$), species are specialists; most species are consuming different resources, and the niche overlap is low. Thus, $M_{\text{consumed}}/M_{\text{total}}$ controls the density of the interactions and could influence the ruggedness of the community landscape.

To gain a broader view of the community structure, we opted not to consider a specific ecological function, but instead looked at the abundances of all species in the community. Thus, we studied the assembly map, $\vec{N}(\vec{\sigma})$, from initial composition to steady-state abundances. Since optimization is easy for linear problems, we quantified the linearity of $\vec{N}(\vec{\sigma})$ by fitting the following model to the data

$$N_i(\vec{\sigma}) = \begin{cases} \sum_{j=1}^S A_{ij}\sigma_j + \epsilon_i, & \text{if } \sigma_i = 1 \\ 0 & \text{if } \sigma_i = 0. \end{cases} \quad (1)$$

where ϵ_i is the model error, and A_{ij} are determined via the least-squares regression.

The differences between the actual and predicted values of the abundance of species i across all possible communities can be used to compute the coefficient of determination R_i^2 . The performance of the linear model in predicting the abundance of all species in the community is then characterized by the average of R_i^2 across all the species. This average $\overline{R^2}$ is close to zero when the linear model fails to fit the data; $\overline{R^2}$ is close to one when the assembly map is approximately linear and species abundances are explained well by independent contributions from other community members.

As expected, Fig. 2 shows that community assembly becomes simpler as the number of interspecific interactions decreases. For low niche overlap, we obtained good linear fits and large values of $\overline{R^2}$. In contrast, $\overline{R^2}$ was small when niche overlap was high. This behavior was consistent across different numbers of candidate species and resources, so we chose the niche overlap as the default method to control community structure. We also checked whether our conclusions are robust by changing environmental complexity or by including metabolic cross-feeding; see the results below and SI Fig. S1.

The role of community function

The optimization process could be affected not only by the interspecific interactions, but also by the community function that is being maximized. To investigate this possibility, we studied the efficacy of the search process for three choices of the community function described below. Since consumer-resource models simplify details of microbial metabolism, we did not explicitly model the production of a desired metabolite. Instead, we followed experimental studies in expressing the desired community function in terms of species abundances in the community [68, 69].

The three community functions were chosen to cover scenarios ranging from functions dependent on the contributions of many species to functions dependent on just a single species. The first community function (diversity) was the diversity of the community. We explored this function

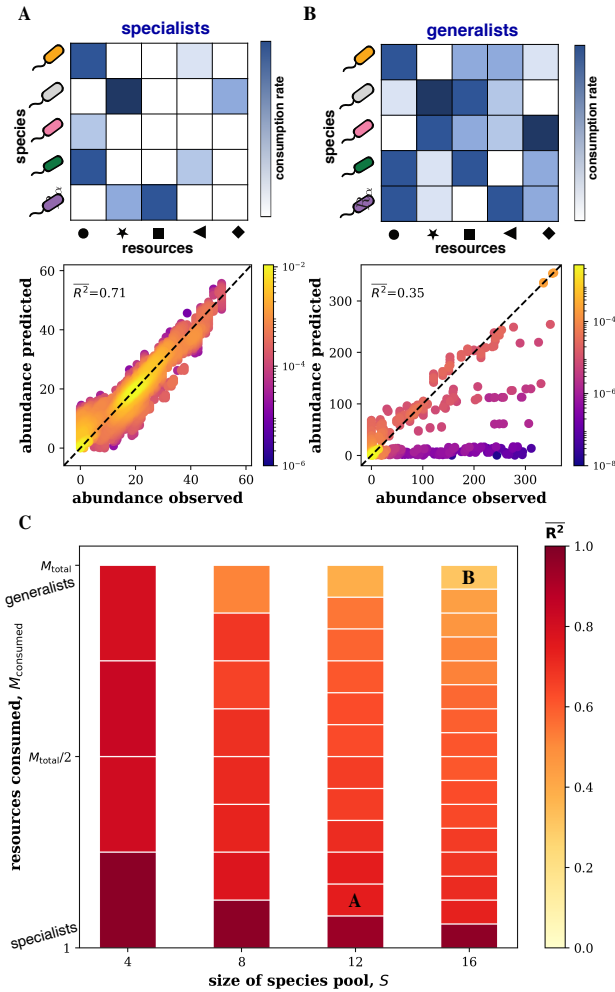


Figure 2: **Niche overlap determines the linearity of ecological landscapes.** The top panels in (A) and (B) show the consumption matrices for species in each species pool. In (A), the niche overlap is low because the species are specialists and consume only a few resources. In (B), the niche overlap is high because the species are generalists and consume many resources. The bottom panels show how well a linear model (Eq. 5) fits the steady-state abundances across all possible species combinations. The goodness of the model fit, quantified by $\overline{R^2}$, is higher when the niche overlap is lower. This conclusion is robust to varying the size of the community and the degree of niche overlap. (C) shows how $\overline{R^2}$ varies with the number of species in the pool, S , and the average number of resources that they consume, M_{consumed} . The degree of niche overlap is determined by $M_{\text{consumed}}/M_{\text{total}}$. Letters indicate the parameters used in panels A and B. Note that $\overline{R^2}$ was computed by averaging R^2 of the linear model fitted separately for each species, and the number of resources supplied was fixed to $M_{\text{total}} = S$. For each set of parameters, results were averaged over 10 independently generated species pools. Other simulation parameters are provided in Methods, and the robustness of the conclusions to certain modeling assumptions is further discussed in the SI.

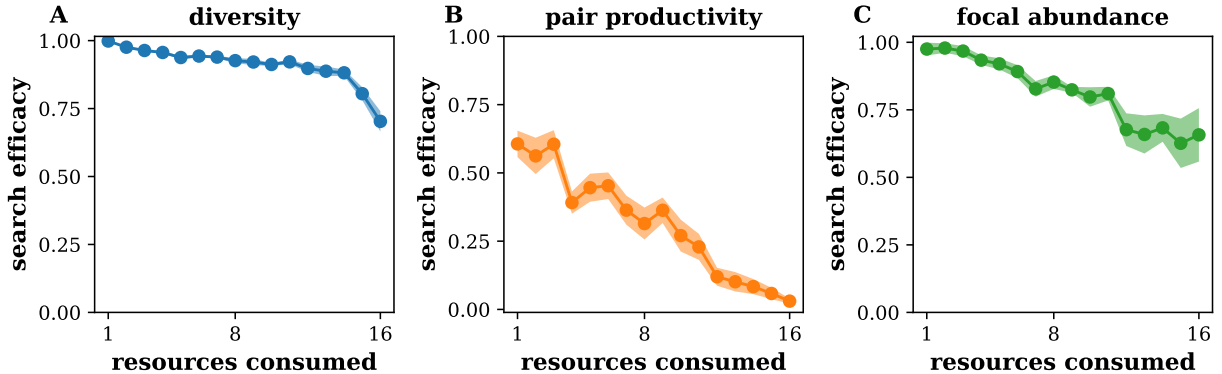


Figure 3: **Search efficacy decreases with niche overlap.** Search efficacy was quantified as the ratio of the best community function found by the search $\mathcal{F}_{\text{found}}$ to the highest value \mathcal{F}_{max} across the entire landscape. The plots report the average and the standard error of the mean obtained from ten independently generated species pools. Different panels correspond to different community functions. The complexity of the landscape was controlled by varying the average number of resources that each species consumed M_{consumed} while keeping the total number of resources M_{total} fixed at $M_{\text{total}} = S = 16$. See Methods for a complete description of these simulations.

because it could be predictive of the overall community productivity in some ecosystems [70–73]. The precise definition of the diversity did not affect our conclusions, so we focused on the Shannon Diversity (Eq. 7). The second community function (pair productivity) was the product of the abundances of two specific microbes (Eq. 8). This choice was motivated by the communities where the combined efforts of two species were necessary to produce a metabolite. The third community function (focal abundance) was simply the abundance of a given species, which could reflect the production or degradation of a specific metabolite.

We quantified the search efficacy as the ratio of the best community function found by the search $\mathcal{F}_{\text{found}}$ to the highest value \mathcal{F}_{max} across the entire landscape. To reduce the influence of the starting community, we report the search efficacy averaged over all possible starting communities.

Qualitatively, the results were the same for all three community functions: The efficacy of search decreased with increasing niche overlap (Fig. 3). We however found important quantitative differences. While optimization of diversity showed only a modest drop with higher niche overlap, the search efficacy for pair productivity plummeted to near zero. This sharp drop was due to sporadic coexistence of the two species. When the two species do not coexist in a region of the landscape, the community function is zero in that neighborhood and the search cannot progress. This challenge can be partly overcome by starting search from the best out of many random communities instead of a single one, which we discuss in Fig. 9.

Ruggedness of ecological landscapes

Niche overlap is only one of many mechanisms that can produce ecological landscapes of varying complexity. For example, cross-feeding could lead to additional interactions not captured by the consumption matrix. It would therefore be quite valuable to develop a mechanism-free metric of landscape complexity. In population genetics and optimization theory, such metrics are known as

landscape ruggedness [74–76]. Rugged landscapes with many scattered peaks are much harder to navigate than smooth landscapes with a single peak. Many measures of ruggedness exist, and some of the most commonly used ones are described in the SI. In the main text, we limit the discussion to the three metrics that we found to be the most useful for microbial communities. These metrics are described below, and their mathematical definitions are provided in Methods.

The roughness-slope ratio r/s quantifies landscape linearity [76, 77]. The roughness, r , measures the error of a linear fit to the community function landscape and the slope, s , measures the average magnitude of the change in \mathcal{F} when a species is added or removed. Small values of r/s indicate that there is a strong trend that is slightly obscured by local fluctuations. Such landscapes are easy to navigate because the heuristic search can detect the direction of the gradient. The exact opposite occurs for large r/s because large point-to-point fluctuations obscure the path towards the optimum.

A related, but different approach is to capture the changes in the community function upon adding or removing a single species. This metric is defined as $1 - Z_{\text{nn}}$, where Z_{nn} is the average correlation between the values of \mathcal{F} in communities that differ by adding or removing a single species. Large values of $1 - Z_{\text{nn}}$ indicate that changes in community function are uncorrelated and the search is difficult.

The third metric, F_{neut} , captures the challenge of quasi-neutral directions. If changes in σ leave the community function nearly the same, then it is difficult to determine how to modify the community to increase \mathcal{F} . This situation occurs when the added species fails to establish or fail to affect the function of interest despite invading. Quasi-neutral directions are common in some landscapes and are known to be a major impediment to optimization [78–80]. Thus, the fraction of quasi-neutral directions F_{neut} could be a valuable predictor of the search success.

We analyzed how these three metrics change with the niche overlap across different community functions. In all cases, we found that landscape ruggedness increases with the number of interspecific interactions. The plots in Fig. 4 are representative of the behavior that we observed. Note that the magnitude and pace of increase varied among the metrics suggesting that there could be important differences in their ability to predict the efficacy of the heuristic search.

We also examined potential limitations of ruggedness metrics. Because they map the entire ecological landscape into a single number, ruggedness measures may not fully capture the actual structure of the search space. Hence, we looked for a ruggedness metric that captures the landscape with more than just a single number. Moreover, we sought to capture nonlinear effects, which are typically ignored by the commonly-used measures of ruggedness. To capture higher-order effects, we examined the fits of $\mathcal{F}(\vec{\sigma})$ by models of increasing complexity. Starting with the linear model, we added quadratic, cubic, quartic, etc terms in $\vec{\sigma}$ (see Methods). These terms account for non-pairwise interactions, e.g. interactions influenced by other species. Such conditional interactions could occur via a variety of mechanisms; for example, a species can induce an interaction between two other species by producing a nutrient that is consumed by both of these other species.

The model errors (unexplained variance) decreased approximately exponentially with the model complexity (Fig. 5). The rate of decrease was similar for smooth and rugged landscapes with rugged landscapes always requiring a more complex model to achieve similar accuracy. We found no compelling examples to justify characterizing landscape ruggedness by more than a single number.

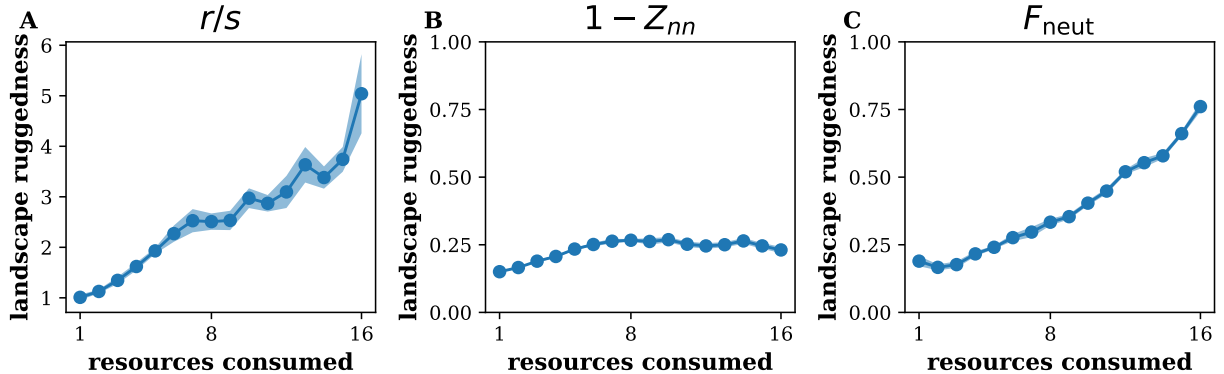


Figure 4: **Ruggedness of community function landscapes.** All metrics of ruggedness increased with niche overlap. Different panels correspond to different metrics of ruggedness. The plots report the average and the standard error of the mean obtained from ten independently generated species pools. The complexity of the landscape was controlled by varying the average number of resources that each species consumed, M_{consumed} , while keeping the total number of resources, M_{total} , fixed at $M_{\text{total}} = S = 16$. See Methods for the complete description of these simulations. The community function here was community diversity; see SI Fig. S2 for another community function.

Therefore, we focused on the simple metrics of landscape ruggedness defined above.

Search is harder on rugged landscapes

Although optimization should be more difficult on rugged landscapes, it is still necessary to quantify this relationship and determine which, if any, of the ruggedness measures can be used in real-world applications. So, we evaluated the search efficacy for the landscapes from Fig. 4. All three ruggedness metrics were significantly anti-correlated with the search efficacy ($p \ll 10^{-4}$).

The examples of these correlations are shown see Fig. 6, which also illustrates how the strength of the correlation varies with the metric and community function. Notably, the roughness-slope ratio consistently showed the strongest anti-correlation, and ruggedness measures were more predictive of functions determined by groups of interacting species. Overall, we found that landscape ruggedness is a good predictor of the search success across all situations examined.

Landscape ruggedness can be estimated from limited data

So far, all of our results were obtained with the full knowledge of the ecological landscape. In practical applications, however, one can examine only a very limited set of species combinations. Thus, it is important to determine whether the ruggedness of a landscape can be determined from limited data.

We estimated different ruggedness metrics for various fractions of the complete landscapes. This was done differently for different metrics because some of them require information on the nearest neighbors while others do not; see Methods. The results showed that ruggedness can indeed be well estimated from as little as 0.1 % of the total number of possible communities (Fig. 7A,B). Moreover, the estimated ruggedness remained highly informative of search success (Fig. 7C). The practical

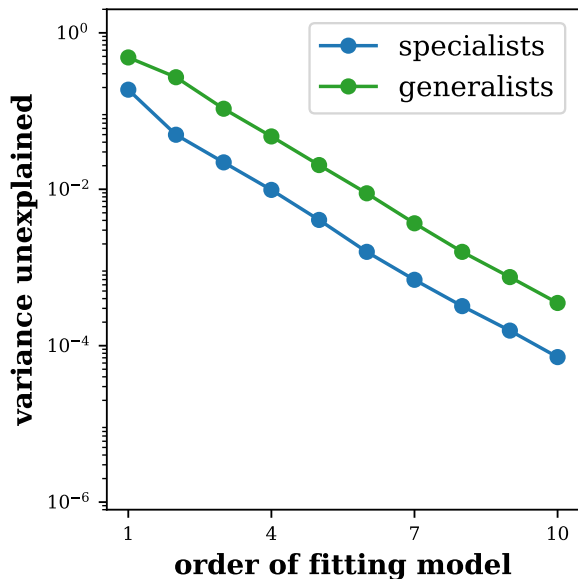


Figure 5: **Contribution of higher-order interactions.** Including higher order terms in the fitting model reduced the variance in the data not explained by the fit. First order fitting models are linear, second—quadratic, etc. The decrease in unexplained variance was approximately exponential. We used $S = 16$, $M_{\text{consumed}} = 2$ for specialists and $M_{\text{consumed}} = 14$ for generalists; the community function was Shannon diversity. All other simulation parameters are the same as in Fig. 4.

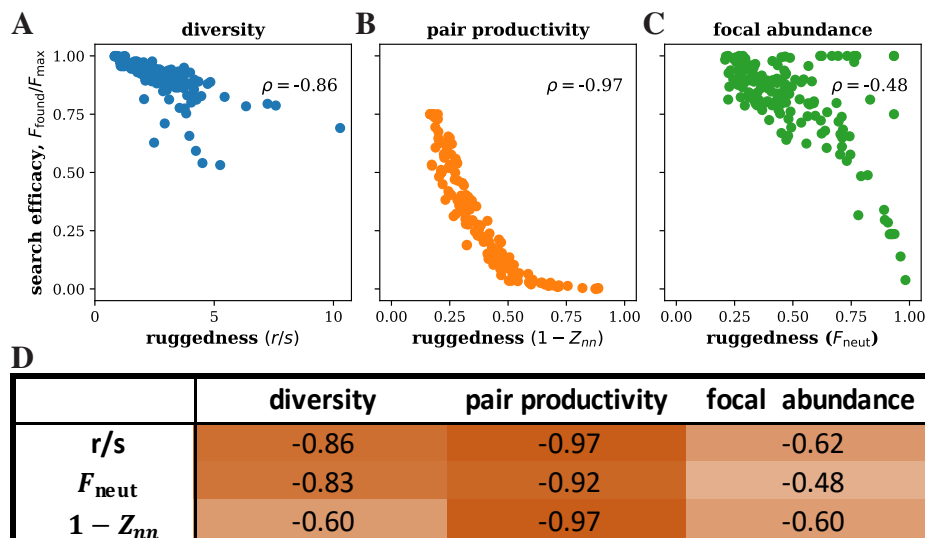


Figure 6: **Landscape ruggedness inhibits search success.** Search efficacy is anti-correlated with the landscape ruggedness. Panels (A), (B), (C) show examples for different community functions and ruggedness metrics. Each point corresponds to a separate $S = 16$ species pool studied in Fig. 4. The systematic effects of the ruggedness metric and the type of community function is explored in (D), which reports the Spearman's correlation coefficient ρ between search efficacy and ruggedness. The correlations were highly significant ($p \ll 10^{-4}$) in all cases.

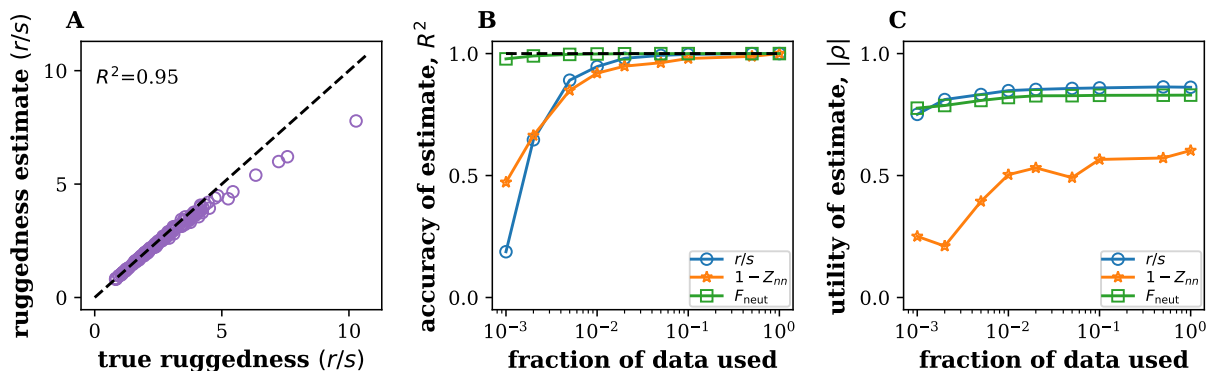


Figure 7: **Estimating ruggedness from limited data.** (A) True and estimated ruggedness are tightly correlated when only 1% of the data is available for the estimation. The data are from Fig. 4, and each point corresponds to a landscape with a different degree of niche overlap. (B) The accuracy of the estimation improves with the amount of available data for all ruggedness measures. (C) The estimated ruggedness remain highly informative of search efficacy. The utility of the ruggedness estimate, $|\rho|$, is measured as the magnitude of the Spearman’s correlation coefficient between search efficacy and estimated ruggedness. Note that $|\rho|$ remained close to one even for very low fractions of the data for which R^2 in panel B started to decrease rapidly suggesting that deviations between predicted and actual roughness (see A and B) do not impede the prediction of search success. For this figure, the community function is the Shannon diversity. Similar results were obtained for other functions tested.

utility of ruggedness estimates was further confirmed by their robustness to the measurement noise (Fig. S3).

Results generalize to other models and search protocols

We further tested the utility of ruggedness measures by applying them to different models and search protocols.

The standard consumer-resource models are undeniably simpler than real microbial communities and have certain mathematical properties that may not hold in more general settings [29, 30]. Since metabolic exchanges are central to most applications [60, 62, 81], we tested the robustness of our results by adding cross-feeding into our model. This was accomplished by specifying the “metabolic leakage matrix” that linked the consumption of each resource to the production of another resource. A certain fraction, l , of the produced resources was allowed to “leak” into the environment, where it could be consumed by all species [32].

First, we checked whether our results still hold when there is a nontrivial amount of leakage. This was indeed the case, and landscape ruggedness was predictive of the search efficacy; see Fig. S4. Then, we examined how leakage affected the community, landscape ruggedness, and search efficacy. Leakage tended to increase the number of surviving species and the diversity of the steady-state communities (Fig. 8A). However, it had no systematic affect on any of the ruggedness measures or search efficacy (Fig. 8A,C). Importantly, when we pooled the simulations across all leakage levels, we still found a strong negative relationship between landscape ruggedness and the

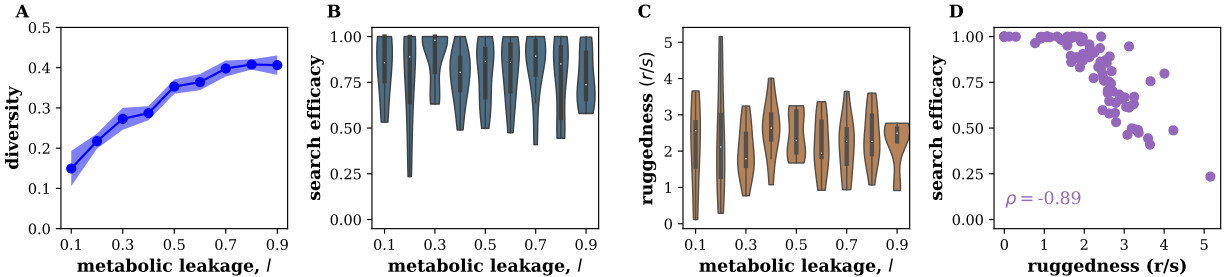


Figure 8: **Ruggedness is predictive of search efficacy in models with cross-feeding.** Cross-feeding altered the composition of microbial communities (A), but had no systematic effect on the success of the heuristic search (B) or ruggedness (C). Importantly, the search efficacy and ruggedness remained strongly anti-correlated in communities with cross-feeding (D). Simulated species pools had $S = 12$ species that leaked a fraction l of the resources they consumed as consumable byproducts. Only one out of 12 modeled resources was supplied externally; the rest were present only due to metabolic leakage. Each species was able to consume 6 resources. Ruggedness was quantified by r/s . Community function used in panels B, C, D is the abundance of a focal species. See Methods for further details.

success of the search (Fig. 8D).

The choice of the search protocol also had no major effect on our conclusions. We considered three variations of the simple gradient-ascent considered so far. The first variation was a simple improvement: instead of starting from a single community, the search commenced from the best of q randomly chosen communities. This procedure helped reduce variability of the search length and avoid really poor outcomes due to an unfortunate starting point. We denote this search protocol ‘one-step reassembly’ as communities at each iteration need to be assembled from scratch using some of the S species.

We also considered two other protocols that mirrored recently proposed community selection methods [82]. These protocols modified the existing community instead of reassembling it from isolates. While adding another species to an existing community is straightforward, removing a species is not. A typical solution of this problem is to perform a strong dilution such that the one or more species become extinct due to the randomness of the dilution process. Our second search protocol was to start from the best of the q communities and then dilute it to create q new communities and $q - 1$ of these new communities are diluted further to promote stochastic extinctions. Then then best community is selected for the next iteration. The third search protocol was the same as the second, except a different random species was added to each of the $q - 1$ strongly diluted communities. We denote these two dilution-based search protocols as ‘bottleneck’ and ‘addition + bottleneck’ respectively.

While the dilution protocols could be appealing, it is worth noting that their performance strongly depended on the dilution factors, which needed to be carefully adjusted for optimal performance. Outside of this narrow range, either too many species went extinct or all species survived (SI Fig. S5). For each protocol, we chose the dilution rate that yielded the best performance. In other words, our results are for the best-case scenario.

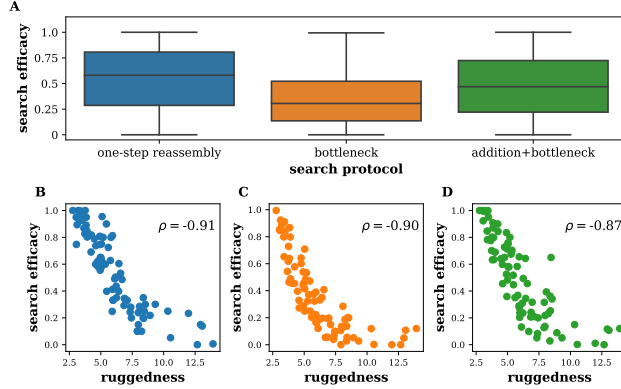


Figure 9: **Ruggedness is informative for a variety of search protocols** (A) shows the search efficacy of three different community optimization protocols. Despite differences in the performance of different protocols, ruggedness remained informative of search success across protocols (panels B, C, D). Community function was pair-productivity. All searches started from the best of $q = 13$ communities. Dilution rate in the dilution-based protocols was adjusted for the highest performance. Simulated communities were the same as in Fig. 8.

The search efficacy differed substantially among protocols. The ‘one-step reassembly’ and ‘addition + bottleneck’ performed best in our tests. Importantly, the difference in performance did not affect the relationship between landscape ruggedness and search efficacy (Fig. 9B,C,D).

Ruggedness of an experimental landscape

We also were able to examine the relationship between landscape ruggedness and search efficacy in an experimental data set. Unfortunately, we found only a single study that had a number of complete ecological landscapes. Langenheder, et. al. [26] measured the metabolic activity of a community of six soil microbes grown on seven different carbon sources in all possible species combinations (Fig. 10).

To check whether these landscape are similar to the ones from consumer-resource models, we determined how well they can be fitted by models of varying complexity (compare to Fig. 5). For all seven experimental landscapes, we found that the accuracy of the fit dramatically improved the complexity of the model and that the quantitative metrics of ruggedness were comparable to those in simulated consumer-resource models (Fig. 10B).

Encouraged by these observations, we computed landscape ruggedness and estimated the performance of the heuristic search. The results are shown in Fig. 10A. In agreement with our expectations, we found that the ruggedness and efficacy were anti-correlated (Spearman’s correlation coefficient, $\rho = -0.46$), but this anti-correlation did not reach statistical significance ($p = 0.29$). The lack of significance could be attributed in part due to the small size of the data set and in part due to the choice of the species and carbon sources. Because of the rather simple metabolic interactions in these communities, the community landscapes were quite smooth and the search efficacy was quite high. Notably, the search efficacy was the highest on the least rugged landscape (xylose), and the search efficacy was perfectly anti-correlated with ruggedness on the three pure carbon sources (Spearman’s correlation coefficient, $\rho = -1$, $p = 0.0$).

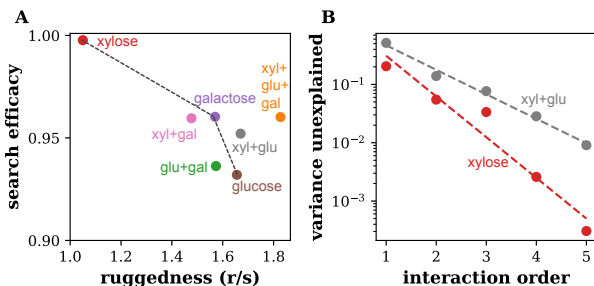


Figure 10: **Ruggedness of experimental landscapes** (A) shows the ruggedness and search efficacy in the seven environments studied in Ref. [26] labeled by the carbon sources used. There is an apparent anticorrelation between the efficacy and ruggedness, but it does not reach statistical significance ($p = 0.29$). Note that the range of ruggedness and search efficacy is quite narrow presumably because of the overlap in the carbon sources in different environments and the choice of species that grow well on these sugars. Nevertheless, the search efficacy is perfectly anti-correlated with ruggedness on the three pure carbon sources (connected by dashed line) and highest on the least rugged landscape (xylose). (B) The decrease in the variance unexplained with increasing model complexity shows behavior similar to that of the simulated landscapes in Fig. 5. Dashed lines in panel B show a linear fit on the semi-logarithmic plot.

Discussion

Many problems in biotechnology can be solved by a well-chosen microbial community. However, designing communities is a challenging and multifaceted process. At the very least, it involves identifying promising candidate species and then sifting through the combination of these species to find a productive and stable community. Since an exhaustive assessment of all possible species combinations is rarely possible, an efficient search protocol is key to the design of microbial communities.

A number of such search protocols have been proposed so far [14, 15, 83, 84]. All of these protocols share the idea of selecting the best performing communities at each stage of the search. However, many of them failed to improve on the best community in the starting pool because they did not modify the selected communities between search stages [82]. Search protocols that modify the selected community at each search stage should fare better. Protocols based on reassembling the community at each stage, like the ones examined here, are a promising way of systematically exploring the space of possible communities.

To uncover the factors controlling the success of search protocols, we introduced the concept of a community function landscape that describes how the community function changes with community composition, in the context of community design. We focused on ecosystems in which the population comes to a unique steady state that is fully determined by the presence-absence of microbes in the starting community. Although such simple dynamics appear to be quite common, there are well-known exceptions (Table 1). Often, these special cases occur only in a limited region of the parameter space and, at a practical level, can be ignored. This simplification allowed us to rigorously define the community function landscape and propose simple measures to characterize its structure.

We found that the success of a heuristic search largely depends on the metrics of landscape ruggedness. Three ruggedness metrics stood out as the most useful: r/s , $1 - Z_{\text{nn}}$, and F_{neut} . The roughness-slope metric, r/s , was the most predictive in our studies, and estimates from limited data remained highly informative of search. The fraction of neutral directions, F_{neut} , was also predictive and easy to estimate, but had an important downside: It required a quantitative threshold for distinguishing neutral directions, which cannot be determined without additional experiments. In practice, the best metric may vary depending on the nature of the ecosystem and experimental constraints.

We also identified how landscape ruggedness depends on the ecology of the microbial community. Our simulations showed that dense networks of metabolic interactions increase the ruggedness of the landscape and reduce the search efficacy. Thus, it could be important to choose the species and environmental variables in a manner that minimizes unnecessary interactions.

While this study relied heavily on consumer-resource models, we expect that our conclusions hold more generally. Indeed, all of our results remained unchanged when various levels of cross-feeding was incorporated in the model. The analysis of experimental landscapes corroborated our conclusions as well.

Ecological landscapes are very versatile because they can be inferred from both simulations and experiments and can even be compared across different ecosystems. Furthermore, landscapes can be reconstructed simply by measuring the community function across different species combinations. In contrast, alternative optimization approaches require sequencing to infer microbial abundances and a mathematical model to predict desired community composition [68, 85–87] or focus on communities with just two species [88–90]. Ecological landscapes may also facilitate the diffusion of knowledge from other disciplines. One such example is the idea of community coalescence that is analogous to recombination in population genetics [91]. In sum, the versatility of ecological landscapes and the practicality of ruggedness metrics can make them a valuable tool for bioengineering applications.

Methods

Consumer-resource models with and without cross-feeding

We simulated a consumer-resource model where species competed for M_{total} resources, which were supplied externally [27, 92]. A species i had abundance n_i , growth rate g_i , and maintenance cost m_i . A resource α had concentration R_α and quality w_α . Resource supply resembled a chemostat with supply point R_α^0 and dilution rate τ^{-1} . Species differed in their preferences for the various resources, encoded in the consumption preference matrix C . A species could consume M_{consumed} randomly chosen resources out of the M_{total} supplied resources. The strength of this preference was randomly drawn from a gamma distribution. The equations governing the dynamics of the species and resources are:

$$\frac{dn_i}{dt} = g_i n_i \left[\sum_{\alpha=1}^M w_\alpha \mu(C_{i\alpha} R_\alpha) - m_i \right], \quad (2)$$

$$\frac{dR_\alpha}{dt} = \tau^{-1} (R_\alpha^0 - R_\alpha) - \sum_{i=1}^S n_i \mu(C_{i\alpha} R_\alpha), \quad (3)$$

where μ is a function describing resource uptake rates. For the consumer resource model without cross-feeding, we assumed a simple linear form for the uptake.

Simulations were carried out in python using custom code and a modified version of the community simulator package [64]. Obtaining the steady state via direct numerical integration of the ODEs is computationally expensive as the number of species combinations grows exponentially with pool size. Therefore, we utilized a recently discovered mapping between ecological models and convex optimization to calculate the steady state quickly [64, 93]. Species with an abundance below 10^{-6} were set to be extinct.

To incorporate the secretion and uptake of metabolites by microbes, we examined the microbial consumer-resource model with cross-feeding [32]. In the cross-feeding model, each species leaks a fraction, l , of resources it consumes in the form of metabolic byproducts. The composition of these byproducts is specified by the metabolic leakage matrix \mathcal{L} , with matrix element $\mathcal{L}_{\alpha\beta}$ specifying the amount of resource β leaked when the species consumes resource α . This leakage is weighted by the ratio of resource qualities w_β/w_α so that energy-poor resources cannot produce a disproportionate amount of energy-rich resources. Each row of the leakage matrix sums to one. The leakage matrix and resource qualities were independent of species identity to respect potential universal stoichiometric constraints on species metabolism. The dynamical equations of the model with cross-feeding are:

$$\begin{aligned} \frac{dn_i}{dt} &= g_i n_i \left[(1-l) \sum_{\alpha=1}^M w_\alpha \mu(C_{i\alpha} R_\alpha) - m_i \right], \\ \frac{dR_\alpha}{dt} &= \tau^{-1} (R_\alpha^0 - R_\alpha) - \sum_{i=1}^S n_i \mu(C_{i\alpha} R_\alpha) + l \sum_{i=1}^S \sum_{\beta=1}^M n_i \mathcal{L}_{\alpha\beta} \frac{w_\beta}{w_\alpha} \mu(C_{i\beta} R_\beta). \end{aligned} \quad (4)$$

Here, resource uptake rates were assumed to be of Monod form, $\mu(x) = x / \left(1 + \frac{x}{K_\alpha}\right)$. We simulated the system of ODEs explicitly using the community simulator package to obtain steady-state abundances. Since direct simulation of the ODEs is computationally expensive, we simulated smaller

candidate species pools with $S = 12$. Simulations reached steady state if the root mean square of the logarithmic species growth rates rates fell below a threshold, i.e., $\text{RMS} \left(\frac{1}{n_i} \frac{dn_i}{dt} \right) < 10^{-3}$. We imposed an abundance cutoff at periodic intervals during the numerical integration to hasten the extinction of species. We verified that the extinct species could not have survived in the community by simulating a re-invasion attempt of the steady-state community.

Simulation parameters

In simulations without cross-feeding, we simulated candidate species pools with S species and supplied M_{total} resources. All species within a candidate species pool consumed a fixed number of resources, M_{consumed} , chosen randomly for each species. The strength of these non-zero consumption preferences were chosen from a gamma distribution with parameters $(k, \theta) = (10, 0.1)$. Growth rates g_i and death rates m_i were sampled from normal distributions with mean 1.0 and variance 0.1 (truncated to ensure positivity). Resource quality w_α and chemostat fixed point R_α^0 were sampled from gamma distributions parameterized by $(k, \theta) = (10, 0.1)$ and $(k, \theta) = (10, 2)$; chemostat dilution rate τ^{-1} was set to 1.

In these simulations, we varied M_{consumed} from 1 resource to M_{total} resources across different candidate pools. We simulated ten pools at each value of M_{consumed} . We examined candidate pools of varying sizes: Figure 2 corresponds to simulations for $(S, M_{\text{total}}) = \{(4, 4), (8, 8), (12, 12), (16, 16)\}$. Figures 4, 5, 6, 7 present data from the 16 species candidate pools. We also simulated and analyzed results for $(S, M_{\text{total}}) = \{(8, 4), (12, 6), (16, 8)\}$ and $(S, M_{\text{total}}) = \{(8, 16), (12, 24), (16, 32)\}$ to verify that our results are robust to the number of supplied resources.

In simulations with cross-feeding (Figs. 8, 9), we simulated $S = 12$ candidate species and $M_{\text{total}} = 12$ resources. Only a single resource, R_0 , was supplied externally. The resource was supplied in sufficient amounts (with a chemostat fixed point $R_0^0 = 240$) that many species were able to survive by feeding on the byproducts of the consumers of the supplied resource. Species leaked a fraction l of the consumed resources in forms specified by the leakage matrix. Each column of the leakage matrix was sampled from a Dirichlet distribution with parameter 0.5. Using the Dirichlet distribution guaranteed that each column summed to one. The Monod form for resource uptake had parameter $K_\alpha = 20$. The chemostat dilution rate was set to 0.1. All other parameters: growth rates g_i , death rates m_i , resource quality w_α , and strength of consumption preferences $C_{i\alpha}$, were sampled as in the consumer-resource model.

We performed three types of simulations with the cross-feeding model—examining the effect of the extent of cross-feeding, environmental complexity, and niche overlap. Parameters were chosen as below:

1. To examine the effect of the extent of cross-feeding, we varied the metabolic leakage fraction l from 0.1 to 0.9 across species pools. The number of resources consumed by each species, M_{consumed} , was 6. To ensure that at least one species in every candidate pool could consume the supplied resource, we constrained species 0 to always consume the sole supplied resource R_0 and species 1 to never consume R_0 . (Both species could still only consume 6 resources in total). The abundance cutoff was 10^{-6} . These simulations are analyzed in Figs. 8, 9.
2. To examine the impact of environmental complexity, we varied the number of resources supplied, R_{supplied} , from 1 to 12 across species pools. We fixed $l = 0.5$ and $M_{\text{consumed}} = 6$. We fixed the

total supply flux of resources by setting the individual resource supply points to $240/R_{\text{supplied}}$. The abundance cutoff was 10^{-3} . Results are shown in SI Fig. S6. Similar results were obtained when we allowed the total resource supply flux to increase with the number of supplied resources (each individual resource had supply point at 240).

3. To examine effect of niche overlap, we vary the number of resources consumed from 1 (extreme specialists) to 12 (extreme generalists). The metabolic leakage fraction was fixed at $l = 0.5$. We constrained species 0 to always consume the sole supplied resource R_0 , to ensure that at least one species ate the supplied resource. The abundance cutoff was 10^{-3} . Results are shown in SI Fig. S4

For each set of parameters, we generated 10 candidate pools differing only by the random sampling.

Characterizing the map to steady-state abundances $\vec{N}(\vec{\sigma})$

Using the simulation models parameterized as above, we simulated all possible combinations of species in the candidate species pools till they reached steady-state. To characterize the assembly map $\vec{N}(\vec{\sigma})$, we quantified how well observed abundance of each species is explained by adding independent contributions from other community members. Therefore, we fit the steady-state abundance of a species i , $N_i(\vec{\sigma})$, using the model

$$N_i(\vec{\sigma}) = \begin{cases} \sum_{j=1}^S A_{ij}\sigma_j + \epsilon, & \text{if } \sigma_i = 1 \\ 0 & \text{if } \sigma_i = 0. \end{cases} \quad (5)$$

where σ_i and σ_j denote the presence-absence of species i and j , A is the matrix of effective interactions, and ϵ is the model error. Note that the model can predict negative abundances, which we set to zero. This truncation did not affect our results.

For each species i , we perform a least squares linear regression to infer the corresponding row (row i) of matrix A using data from communities where the species was initially present ($\sigma_i = 1$).

The abundance predicted by the model, $\hat{N}_i(\vec{\sigma})$, is given by

$$\hat{N}_i(\vec{\sigma}) = \begin{cases} \sum_{j=1}^S A_{ij}\sigma_j & \text{if } \sigma_i = 1 \\ 0 & \text{if } \sigma_i = 0. \end{cases} \quad (6)$$

We record the fraction of the variance explained (equivalent to the coefficient of determination) by the model, and repeat the regression for each of the S species. The average variance explained across all S species, $\overline{R^2}$, is a measure of the linearity of the abundance landscape. Results are presented in Fig. 2.

Community function landscapes

We computed the community function of interest, \mathcal{F} , from the steady-state species abundances. The three forms of community functions we analyzed are:

1. Shannon Diversity was measured as

$$\text{diversity} = \frac{1}{\ln S} \sum_{i=1}^S p_i \ln p_i, \quad (7)$$

where p_i is the relative abundance of species i .

2. Pair Productivity, mediated by a pair of species (A, B), was measured as the product of their abundances,

$$\text{pair productivity} = N_A N_B. \quad (8)$$

This approximates a scenario where a useful product is synthesized by the combined activity of two species.

3. Focal abundance. The abundance of a focal species of interest was given by N_{focal} . Since this function makes sense only if the species was present in the initial community, we restricted our analyses to the subset of the complete landscape where the focal species was initially present. This subset resembles a landscape made by $S - 1$ species, with 2^{S-1} species combinations.

Landscape ruggedness

We used three ruggedness measures to characterize the community function landscapes:

1. The roughness-slope ratio r/s is given by the ratio of roughness r to slope s of the landscape. The roughness, r , measures the root-mean-squared residual of the linear fit. It is obtained by fitting the community function \mathcal{F} with the linear model, $\hat{\mathcal{F}}(\vec{\sigma}) = c + \sum_{i=1}^S a_i \sigma_i$, via least squares regression. r is given by

$$r = \sqrt{\frac{1}{\|\vec{\sigma}\|} \sum_{\vec{\sigma}} (\mathcal{F}(\vec{\sigma}) - \hat{\mathcal{F}}(\vec{\sigma}))^2}, \quad (9)$$

where $\|\vec{\sigma}\|$ is the number of points on the landscape.

The slope, s , measures the magnitude of change in \mathcal{F} when a species is added or removed. It is given by

$$s = \frac{1}{S} \sum_{i=1}^S |a_i|. \quad (10)$$

2. $1 - Z_{nn}$, where Z_{nn} is nearest neighbor correlation on the landscape. Z_{nn} is defined as :

$$Z_{nn} = \frac{\frac{1}{\|\vec{\sigma}^{nn}\|} \sum_{\vec{\sigma}, \vec{\sigma}^{nn}} \mathcal{F}(\vec{\sigma}) \mathcal{F}(\vec{\sigma}^{nn}) - \bar{\mathcal{F}}^2}{\sum_{\vec{\sigma}} (\mathcal{F}(\vec{\sigma}) - \bar{\mathcal{F}})^2}. \quad (11)$$

$\vec{\sigma}^{nn}$ refers to the nearest neighbors of $\vec{\sigma}$ on the landscape, i.e., communities obtained by adding or removing a single species, and $\|\vec{\sigma}^{nn}\|$ is the number of nearest neighbors.

3. The fraction of quasi-neutral directions F_{neut} is a third measure of ruggedness. It was measured by computing the fraction of nearest neighbors on the landscape with function values that differed by less than a defined threshold (10^{-4}).

Variance unexplained by higher-order models

We fit ecological landscapes of community function $\mathcal{F}(\vec{\sigma})$ incorporating higher-order species interactions using the following class of models:

$$\hat{\mathcal{F}}^{(k)}(\vec{\sigma}) = a^{(0)} + \sum_{i=1}^S a_i^{(1)} \sigma_i + \sum_{i=1}^S \sum_{j=1}^{i-1} a_{ij}^{(2)} \sigma_i \sigma_j + \dots \mathcal{O}\left(a^{(k)}\right) + \epsilon(\vec{\sigma}), \quad (12)$$

where the fit coefficients $a^{(0)}, a^{(1)}, \dots$ defined up to order k are obtained by least squares regression minimizing $(\hat{\mathcal{F}}^{(k)}(\vec{\sigma}) - \mathcal{F}(\vec{\sigma}))^2$. (Note that we can still use linear regression because the models are linear in the interaction coefficients.)

The fraction of variance unexplained by the model of order k , $U^{(k)}$, is given by

$$U^{(k)} = 1 - \frac{\sum_{\vec{\sigma}} (\hat{\mathcal{F}}^{(k)}(\vec{\sigma}) - \bar{\mathcal{F}})^2}{\sum_{\vec{\sigma}} (\mathcal{F}(\vec{\sigma}) - \bar{\mathcal{F}})^2} \quad (13)$$

where $\bar{\mathcal{F}}$ is the mean function; the numerator and denominator are the explained sum of squares and total sum of squares respectively. The number of higher order terms grows exponentially with the number of species, and so inverting matrices for linear regression became computationally expensive for large landscapes. Therefore, we used an alternative method to calculate the fraction of variance unexplained for large landscapes based on Walsh decomposition (see SI).

We imposed a threshold of 10^{-6} in the fraction of variance unexplained when plotting and fitting data in Fig. 5 to be robust to numerical artifacts.

Heuristic search protocols

We simulated community optimization attempts via a number of different search protocols.

Heuristic gradient-ascent search and one-step reassembly

The gradient-ascent search proceeds as follows:

1. Choose a starting point on the landscape A , with initial composition $\vec{\sigma}^A$ and community function $\mathcal{F}(\vec{\sigma}^A)$.
2. Evaluate the relative change in steady-state community function at all points a single step away on the landscape, i.e, communities obtained by adding or removing a single species to the initial composition at A .

$$\Delta^B = \frac{\mathcal{F}(\vec{\sigma}^B) - \mathcal{F}(\vec{\sigma}^A)}{\mathcal{F}(\vec{\sigma}^A)}, \quad \forall B : |\vec{\sigma}^B - \vec{\sigma}^A| = 1. \quad (14)$$

3. If the community function increased for any of the neighboring communities ($\Delta^B > 10^{-4}$), then we choose the neighboring point with highest community function and repeat from step 2 with this chosen community as A .
4. If the community function did not increase at any neighboring community, the search terminates. The current community is the community found by the search.

In Fig. 9, we study a modified protocol, ‘one-step reassembly’ where search started from the best point out of q randomly chosen communities. We also simulated a version of gradient-ascent search

where search proceeded along the *first* direction with increasing community function (instead of the direction with maximal increase in community function). Similar results were obtained for this version and we omit discussion of these results for brevity.

‘bottleneck’ protocol

The ‘bottleneck’ protocol proceeds as follows:

1. Grow q random communities till steady state. Choose the community with highest function as the starting community.
2. q replicates of the chosen community are generated.
3. $q - 1$ replicates are passaged via severe dilution shocks to generate stochastic species extinctions. One replicate is left unperturbed.
4. The q communities are grown to steady state, and the community with the highest function is chosen.
5. Repeat steps 2-4 for a fixed number of iterations. The best community among the q communities in the last iteration is the community found by the search protocol.

To simulate a dilution shock, the number of cells in the community n_{cells} was first calculated by dividing by a fixed biomass conversion factor of 10^{-3} . The number of cells in the community after dilution by factor D was sampled from a Poisson distribution with mean Dn_{cells} . The number of cells of each species was then obtained by multinomial sampling with probabilities proportional to the biomass of each species.

‘addition + bottleneck’ protocol

The ‘addition + bottleneck’ protocol closely follows the ‘bottleneck’ protocol above, with a single modification. In Step 3, after $q - 1$ replicates are subject to severe dilution shocks, a different randomly chosen species is added to each of these replicates. The q^{th} replicate is still left unperturbed.

We simulated both dilution-based protocols (‘bottleneck’ and ‘addition + bottleneck’) for a range of dilution factors. The two strategies performed best at an intermediate dilution, where dilution stochastically eliminates a few species from the community, but not too many species (Fig. S5). We report the results for the dilution factor that had the highest search efficacy in the main text (Fig. 9).

To ensure a fair comparison between the dilution-based protocols and one-step reassembly, we fixed the number of replicates to $q = S + 1$ and the number of iterations to $S/2$ in the dilution-based protocols, and started one-step reassembly from the best of q random communities in Fig. 9. This ensured that the number of experiments in all strategies were similar.

Search efficacy of all search protocols was evaluated as the ratio between the community function at the end point of the search and the best community function on the landscape. We report search efficacy averaged over all possible starting points on the landscape in figures on the simple gradient-ascent search protocol. In Fig. 9, which compared the dilution-based protocols and ‘one-step reassembly’ we report the search efficacy averaged over 10 independent searches on each landscape.

Sampling ecological landscapes

We estimated ruggedness measures from appropriately sampled subsets of the community function landscapes. To estimate r/s , we randomly sampled a fraction, f , of the possible 2^S communities. The linear model was fit on the sampled data points to estimate r/s . Since the model has $S + 1$ parameters, we need to sample at least $S + 1$ points. To estimate $1 - Z_{nn}$ and F_{neut} , we sampled a fraction f of all communities by choosing half of the communities randomly and generating one random nearest neighbor for each of them. $1 - Z_{nn}$ and F_{neut} were then calculated from the sampled points.

Analysis of experimental data

The experiments by Langenheder, et. al. measured the time series of cumulative metabolic activity, through the intensity of a dye, for each community and environment [26]. We obtained the rate of metabolic activity from the data via a linear fit of the metabolic activity over the last six time points. The communities had reached a steady state in metabolic activity, as evidenced by the high R^2 of the linear fits (SI Fig. S7). We analyzed the landscape formed by the steady-state metabolic rate in Fig. 10. We imposed a threshold in the fraction of variance unexplained (10^{-4}) when plotting and fitting data in Fig. 10B.

Acknowledgments

The authors would like to thank Pankaj Mehta, Gabriel Birzu, Shreya Arya, and James O’Dwyer for helpful discussions and comments, and Silke Langenheder for sharing experimental data. This work was supported by the Simons Foundation Grant #409704, Cottrell Scholar Award #24010, and by NIGMS grant #1R01GM138530-01 to K.S.K. Simulations were carried out on the Boston University Shared Computing Cluster.

References

- [1] Paerl, H. & Pinckney, J. A mini-review of microbial consortia: Their roles in aquatic production and biogeochemical cycling. *Microbial Ecology* **31** (1996). URL <http://link.springer.com/10.1007/BF00171569>.
- [2] Falkowski, P. G., Fenchel, T. & Delong, E. F. The Microbial Engines That Drive Earth’s Biogeochemical Cycles. *Science* **320**, 1034–1039 (2008). URL <https://www.sciencemag.org/lookup/doi/10.1126/science.1153213>.
- [3] Flint, H. J., Scott, K. P., Duncan, S. H., Louis, P. & Forano, E. Microbial degradation of complex carbohydrates in the gut. *Gut Microbes* **3**, 289–306 (2012). URL <http://www.tandfonline.com/doi/abs/10.4161/gmic.19897>.
- [4] Brenner, K., You, L. & Arnold, F. H. Engineering microbial consortia: a new frontier in synthetic biology. *Trends in Biotechnology* **26**, 483–489 (2008). URL <https://linkinghub.elsevier.com/retrieve/pii/S0167779908001716>.
- [5] Olle, B. Medicines from microbiota. *Nature Biotechnology* **31**, 309–315 (2013). URL <http://www.nature.com/articles/nbt.2548>.

- [6] Lindemann, S. R. *et al.* Engineering microbial consortia for controllable outputs. *The ISME Journal* **10**, 2077–2084 (2016). URL <http://www.nature.com/articles/ismej201626>.
- [7] Minty, J. J. *et al.* Design and characterization of synthetic fungal-bacterial consortia for direct production of isobutanol from cellulosic biomass. *Proceedings of the National Academy of Sciences* **110**, 14592–14597 (2013). URL <http://www.pnas.org/lookup/doi/10.1073/pnas.1218447110>.
- [8] Tanoue, T. *et al.* A defined commensal consortium elicits CD8 T cells and anti-cancer immunity. *Nature* **565**, 600–605 (2019). URL <http://www.nature.com/articles/s41586-019-0878-z>.
- [9] Buffie, C. G. *et al.* Precision microbiome reconstitution restores bile acid mediated resistance to *Clostridium difficile*. *Nature* **517**, 205–208 (2015). URL <http://www.nature.com/articles/nature13828>.
- [10] Hu, J. *et al.* Design and composition of synthetic fungal-bacterial microbial consortia that improve lignocellulolytic enzyme activity. *Bioresour Technol* **227**, 247–255 (2017). URL <https://linkinghub.elsevier.com/retrieve/pii/S096085241631728X>.
- [11] Stein, R. R. *et al.* Computer-guided design of optimal microbial consortia for immune system modulation. *eLife* **7** (2018). URL <https://elifesciences.org/articles/30916>.
- [12] Kehe, J. *et al.* Massively parallel screening of synthetic microbial communities. *Proceedings of the National Academy of Sciences* **116**, 12804–12809 (2019). URL <http://www.pnas.org/lookup/doi/10.1073/pnas.1900102116>.
- [13] Villa, M. M. *et al.* High-throughput isolation and culture of human gut bacteria with droplet microfluidics. *bioRxiv* (2019). URL <http://biorxiv.org/lookup/doi/10.1101/630822>.
- [14] Swenson, W., Arendt, J. & Wilson, D. S. Artificial selection of microbial ecosystems for 3-chloroaniline biodegradation. *Environmental Microbiology* **2**, 564–571 (2000). URL <http://doi.wiley.com/10.1046/j.1462-2920.2000.00140.x>.
- [15] Chang, C.-Y., Osborne, M. L., Bajic, D. & Sanchez, A. Artificially selecting microbial communities using propagule strategies. preprint, *Evolutionary Biology* (2020). URL <http://biorxiv.org/lookup/doi/10.1101/2020.05.01.066282>.
- [16] Eng, A. & Borenstein, E. Microbial community design: methods, applications, and opportunities. *Current Opinion in Biotechnology* **58**, 117–128 (2019). URL <https://linkinghub.elsevier.com/retrieve/pii/S0958166918301927>.
- [17] Chen, Y., Lin, C.-J., Jones, G., Fu, S. & Zhan, H. Enhancing biodegradation of wastewater by microbial consortia with fractional factorial design. *Journal of Hazardous Materials* **171**, 948–953 (2009). URL <https://linkinghub.elsevier.com/retrieve/pii/S0304389409010255>.
- [18] Tsoi, R., Dai, Z. & You, L. Emerging strategies for engineering microbial communities. *Biotechnology Advances* **37**, 107372 (2019). URL <https://linkinghub.elsevier.com/retrieve/pii/S0734975019300473>.
- [19] Hsu, R. H. *et al.* Microbial Interaction Network Inference in Microfluidic Droplets. *Cell Systems* **9**, 229–242.e4 (2019). URL <https://linkinghub.elsevier.com/retrieve/pii/S2405471219302315>.

- [20] Zanakis, S. H. & Evans, J. R. Heuristic “Optimization”: Why, When, and How to Use It. *Interfaces* **11**, 84–91 (1981). URL <http://pubsonline.informs.org/doi/abs/10.1287/inte.11.5.84>.
- [21] Rardin, R. L. & Uzsoy, R. Experimental Evaluation of Heuristic Optimization Algorithms: A Tutorial. *Journal of Heuristics* 261–304 (2001).
- [22] Marsland III, R., Cui, W. & Mehta, P. A minimal model for microbial biodiversity can reproduce experimentally observed ecological patterns. *arXiv:1904.12914 [physics, q-bio]* (2019). URL <http://arxiv.org/abs/1904.12914>. ArXiv: 1904.12914.
- [23] Ho, P.-Y., Good, B. & Huang, K. C. Competition for fluctuating resources reproduces statistics of species abundance over time across wide-ranging microbiotas. preprint, *Ecology* (2021). URL <http://biorxiv.org/lookup/doi/10.1101/2021.05.13.444061>.
- [24] Gowda, K., Ping, D., Mani, M. & Kuehn, S. A sparse mapping of structure to function in microbial communities. preprint, *Ecology* (2020). URL <http://biorxiv.org/lookup/doi/10.1101/2020.09.29.315713>.
- [25] Wright, S. The roles of mutation, inbreeding, crossbreeding, and selection in evolution. *Proc. VIth Int. Congress of Genetics* **1**, 356–366 (1932).
- [26] Langenheder, S., Bulling, M. T., Solan, M. & Prosser, J. I. Bacterial Biodiversity-Ecosystem Functioning Relations Are Modified by Environmental Complexity. *PLoS ONE* **5**, e10834 (2010). URL <https://dx.plos.org/10.1371/journal.pone.0010834>.
- [27] MacArthur, R. Species packing and competitive equilibrium for many species. *Theoretical Population Biology* **1**, 1–11 (1970). URL <https://linkinghub.elsevier.com/retrieve/pii/0040580970900390>.
- [28] Armstrong, R. A. & McGehee, R. Competitive Exclusion. *The American Naturalist* **115**, 151–170 (1980). URL <http://www.jstor.org/stable/2460592>. Publisher: [University of Chicago Press, American Society of Naturalists].
- [29] Tikhonov, M. Community-level cohesion without cooperation. *eLife* **5**, e15747 (2016). URL <https://elifesciences.org/articles/15747>.
- [30] Marsland III, R., Cui, W. & Mehta, P. The Minimum Environmental Perturbation Principle: A New Perspective on Niche Theory. *arXiv:1901.09673 [physics, q-bio]* (2019). URL <http://arxiv.org/abs/1901.09673>. ArXiv: 1901.09673.
- [31] Ispolatov, I. & Doebeli, M. A note on the complexity of evolutionary dynamics in a classic consumer-resource model. *Theoretical Ecology* (2019). URL <http://link.springer.com/10.1007/s12080-019-0427-2>.
- [32] Marsland, R. *et al.* Available energy fluxes drive a transition in the diversity, stability, and functional structure of microbial communities. *PLOS Computational Biology* **15**, e1006793 (2019). URL <http://dx.plos.org/10.1371/journal.pcbi.1006793>.
- [33] Butler, S. & O’Dwyer, J. P. Stability criteria for complex microbial communities. *Nature Communications* **9** (2018). URL <http://www.nature.com/articles/s41467-018-05308-z>.

- [34] Roy, F., Biroli, G., Bunin, G. & Cammarota, C. Numerical implementation of dynamical mean field theory for disordered systems: application to the Lotka-Volterra model of ecosystems. *arXiv:1901.10036 [cond-mat, q-bio]* (2019). URL <http://arxiv.org/abs/1901.10036>. ArXiv: 1901.10036.
- [35] Kessler, D. A. & Shnerb, N. M. Generalized model of island biodiversity. *Physical Review E* **91** (2015). URL <https://link.aps.org/doi/10.1103/PhysRevE.91.042705>.
- [36] Smillie, J. Competitive and Cooperative Tridiagonal Systems of Differential Equations. *SIAM Journal on Mathematical Analysis* **15**, 530–534 (1984). URL <http://epubs.siam.org/doi/10.1137/0515040>.
- [37] Smith, H. L. Competing Subcommunities of Mutualists and a Generalized Kamke Theorem. *SIAM Journal on Applied Mathematics* **46**, 856–874 (1986). URL <http://epubs.siam.org/doi/10.1137/0146052>.
- [38] Bunin, G. Directionality and community-level selection. *bioRxiv* (2018). URL <http://biorxiv.org/lookup/doi/10.1101/484576>.
- [39] Gibson, T. E., Bashan, A., Cao, H.-T., Weiss, S. T. & Liu, Y.-Y. On the Origins and Control of Community Types in the Human Microbiome. *PLOS Computational Biology* **12**, e1004688 (2016). URL <https://dx.plos.org/10.1371/journal.pcbi.1004688>.
- [40] Vanwonterghem, I. *et al.* Deterministic processes guide long-term synchronised population dynamics in replicate anaerobic digesters. *The ISME Journal* **8**, 2015–2028 (2014). URL <http://www.nature.com/articles/ismej201450>.
- [41] Aranda-Díaz, A. *et al.* High-throughput cultivation of stable, diverse, fecal-derived microbial communities to model the intestinal microbiota. preprint, Microbiology (2020). URL <http://biorxiv.org/lookup/doi/10.1101/2020.07.06.190181>.
- [42] Lucas, R., Kuchenbuch, A., Fetzer, I., Harms, H. & Kleinstuber, S. Long-term monitoring reveals stable and remarkably similar microbial communities in parallel full-scale biogas reactors digesting energy crops. *FEMS Microbiology Ecology* **91** (2015). URL <https://academic.oup.com/femsec/article-lookup/doi/10.1093/femsec/fiv004>.
- [43] Dubinkina, V., Fridman, Y., Pandey, P. P. & Maslov, S. Multistability and regime shifts in microbial communities explained by competition for essential nutrients. *eLife* **8** (2019). URL <https://elifesciences.org/articles/49720>.
- [44] Wang, Z. *et al.* Complementary resource preferences spontaneously emerge in diauxic microbial communities. *Nature Communications* **12**, 6661 (2021). URL <https://www.nature.com/articles/s41467-021-27023-y>.
- [45] Friedman, J., Higgins, L. M. & Gore, J. Community structure follows simple assembly rules in microbial microcosms. *Nature Ecology & Evolution* **1** (2017). URL <http://www.nature.com/articles/s41559-017-0109>.
- [46] Estrela, S. *et al.* Functional attractors in microbial community assembly. *Cell Systems* S2405471221003793 (2021). URL <https://linkinghub.elsevier.com/retrieve/pii/S2405471221003793>.

- [47] Fukami, T., Martijn Bezemer, T., Mortimer, S. R. & Putten, W. H. Species divergence and trait convergence in experimental plant community assembly. *Ecology Letters* **8**, 1283–1290 (2005). URL <http://doi.wiley.com/10.1111/j.1461-0248.2005.00829.x>.
- [48] Louca, S. *et al.* High taxonomic variability despite stable functional structure across microbial communities. *Nature Ecology & Evolution* **1** (2017). URL <http://www.nature.com/articles/s41559-016-0015>.
- [49] Hubbell, S. P. *The unified neutral theory of biodiversity and biogeography*. No. 32 in Monographs in population biology (Princeton University Press, Princeton, 2001).
- [50] Maslov, S. & Sneppen, K. Population cycles and species diversity in dynamic Kill-the-Winner model of microbial ecosystems. *Scientific Reports* **7** (2017). URL <http://www.nature.com/articles/srep39642>.
- [51] Huisman, J. & Weissing, F. J. BIOLOGICAL CONDITIONS FOR OSCILLATIONS AND CHAOS GENERATED BY MULTISPECIES COMPETITION. *Ecology* **82**, 2682–2695 (2001). URL [http://doi.wiley.com/10.1890/0012-9658\(2001\)082\[2682:BCF0AC\]2.0.CO;2](http://doi.wiley.com/10.1890/0012-9658(2001)082[2682:BCF0AC]2.0.CO;2).
- [52] Pearce, M., Agarwala, A. & Fisher, D. S. Stabilization of extensive fine-scale diversity by spatio-temporal chaos. *bioRxiv* (2019). URL <http://biorxiv.org/lookup/doi/10.1101/736215>.
- [53] Ofiteru, I. D. *et al.* Combined niche and neutral effects in a microbial wastewater treatment community. *Proceedings of the National Academy of Sciences* **107**, 15345–15350 (2010). URL <http://www.pnas.org/cgi/doi/10.1073/pnas.1000604107>.
- [54] Samuels, C. L. & Drake, J. A. Divergent perspectives on community convergence. *Trends in Ecology & Evolution* **12**, 427–432 (1997). URL <https://linkinghub.elsevier.com/retrieve/pii/S0169534797011828>.
- [55] Momeni, B., Xie, L. & Shou, W. Lotka-Volterra pairwise modeling fails to capture diverse pairwise microbial interactions. *eLife* **6**, e25051 (2017). URL <https://elifesciences.org/articles/25051>.
- [56] O’Dwyer, J. P. Whence Lotka-Volterra?: Conservation laws and integrable systems in ecology. *Theoretical Ecology* **11**, 441–452 (2018). URL <http://link.springer.com/10.1007/s12080-018-0377-0>.
- [57] Hoek, T. A. *et al.* Resource Availability Modulates the Cooperative and Competitive Nature of a Microbial Cross-Feeding Mutualism. *PLOS Biology* **14**, e1002540 (2016). URL <https://dx.plos.org/10.1371/journal.pbio.1002540>.
- [58] Gopalakrishnappa, C., Gowda, K., Prabhakara, K. & Kuehn, S. An ensemble approach to the structure-function problem in microbial communities. *arXiv:2111.06279 [q-bio]* (2021). URL <http://arxiv.org/abs/2111.06279>. ArXiv: 2111.06279.
- [59] Niehaus, L. *et al.* Microbial coexistence through chemical-mediated interactions. *Nature Communications* **10**, 2052 (2019). URL <http://www.nature.com/articles/s41467-019-10062-x>.

- [60] D’Souza, G. *et al.* Ecology and evolution of metabolic cross-feeding interactions in bacteria. *Natural Product Reports* **35**, 455–488 (2018). URL <http://xlink.rsc.org/?DOI=C8NP00009C>.
- [61] Pacheco, A. R., Moel, M. & Segrè, D. Costless metabolic secretions as drivers of interspecies interactions in microbial ecosystems. *Nature Communications* **10** (2019). URL <http://www.nature.com/articles/s41467-018-07946-9>.
- [62] Datta, M. S., Sliwerska, E., Gore, J., Polz, M. F. & Cordero, O. X. Microbial interactions lead to rapid micro-scale successions on model marine particles. *Nature Communications* **7**, 11965 (2016). URL <http://www.nature.com/articles/ncomms11965>.
- [63] Gralka, M., Szabo, R., Stocker, R. & Cordero, O. X. Trophic Interactions and the Drivers of Microbial Community Assembly. *Current Biology* **30**, R1176–R1188 (2020). URL <https://linkinghub.elsevier.com/retrieve/pii/S0960982220311611>.
- [64] Marsland, R., Cui, W., Goldford, J. & Mehta, P. The Community Simulator: A Python package for microbial ecology. *bioRxiv* (2019). URL <http://biorxiv.org/lookup/doi/10.1101/613836>.
- [65] Hang-Kwang, L. & Pimm, S. L. The Assembly of Ecological Communities: A Minimalist Approach. *The Journal of Animal Ecology* **62**, 749 (1993). URL <https://www.jstor.org/stable/5394?origin=crossref>.
- [66] Morton, R. D., Law, R., Pimm, S. L. & Drake, J. A. On Models for Assembling Ecological Communities. *Oikos* **75**, 493 (1996). URL <https://www.jstor.org/stable/3545891?origin=crossref>.
- [67] Bittleston, L. S., Gralka, M., Leventhal, G. E., Mizrahi, I. & Cordero, O. X. Context-dependent dynamics lead to the assembly of functionally distinct microbial communities. *Nature Communications* **11**, 1440 (2020). URL <http://www.nature.com/articles/s41467-020-15169-0>.
- [68] Clark, R. L. *et al.* Design of synthetic human gut microbiome assembly and butyrate production. *Nature Communications* **12**, 3254 (2021). URL <http://www.nature.com/articles/s41467-021-22938-y>.
- [69] Sanchez-Gorostiaga, A., Bajić, D., Osborne, M. L., Poyatos, J. F. & Sanchez, A. High-order interactions distort the functional landscape of microbial consortia. *PLOS Biology* **17**, e3000550 (2019). URL <https://dx.plos.org/10.1371/journal.pbio.3000550>.
- [70] Diagne, N. *et al.* Ectomycorrhizal diversity enhances growth and nitrogen fixation of *Acacia mangium* seedlings. *Soil Biology and Biochemistry* **57**, 468–476 (2013). URL <https://linkinghub.elsevier.com/retrieve/pii/S0038071712003434>.
- [71] Laforest-Lapointe, I., Paquette, A., Messier, C. & Kembel, S. W. Leaf bacterial diversity mediates plant diversity and ecosystem function relationships. *Nature* **546**, 145–147 (2017). URL <http://www.nature.com/articles/nature22399>.
- [72] Shurin, J. B., Mandal, S. & Abbott, R. L. Trait diversity enhances yield in algal biofuel assemblages. *Journal of Applied Ecology* **51**, 603–611 (2014). URL <http://doi.wiley.com/10.1111/1365-2664.12242>.

- [73] Georgianna, D. R. & Mayfield, S. P. Exploiting diversity and synthetic biology for the production of algal biofuels. *Nature* **488**, 329–335 (2012). URL <http://www.nature.com/articles/nature11479>.
- [74] Stadler, P. F. Landscapes and their correlation functions. *Journal of Mathematical Chemistry* **20**, 1–45 (1996). URL <http://link.springer.com/10.1007/BF01165154>.
- [75] Merz, P. Advanced Fitness Landscape Analysis and the Performance of Memetic Algorithms. *Evolutionary Computation* **12**, 303–325 (2004). URL <https://direct.mit.edu/evco/article/12/3/303-325/1178>.
- [76] Szendro, I. G., Schenk, M. F., Franke, J., Krug, J. & de Visser, J. A. G. M. Quantitative analyses of empirical fitness landscapes. *Journal of Statistical Mechanics: Theory and Experiment* **2013**, P01005 (2013). URL <http://stacks.iop.org/1742-5468/2013/i=01/a=P01005?key=crossref.80c01de42bec35cf69596036ffc8d086>.
- [77] Aita, T., Iwakura, M. & Husimi, Y. A cross-section of the fitness landscape of dihydrofolate reductase. *Protein Engineering, Design and Selection* **14**, 633–638 (2001). URL <https://academic.oup.com/peds/article-lookup/doi/10.1093/protein/14.9.633>.
- [78] Bray, A. J. & Dean, D. S. The statistics of critical points of Gaussian fields on large-dimensional spaces. *Physical Review Letters* **98**, 150201 (2007). URL <http://arxiv.org/abs/cond-mat/0611023>. ArXiv: cond-mat/0611023.
- [79] Fyodorov, Y. V. & Williams, I. Replica Symmetry Breaking Condition Exposed by Random Matrix Calculation of Landscape Complexity. *arXiv:cond-mat/0702601* (2007). URL <http://arxiv.org/abs/cond-mat/0702601>. ArXiv: cond-mat/0702601.
- [80] Dauphin, Y. *et al.* Identifying and attacking the saddle point problem in high-dimensional non-convex optimization. *arXiv:1406.2572 [cs, math, stat]* (2014). URL <http://arxiv.org/abs/1406.2572>. ArXiv: 1406.2572.
- [81] Goldford, J. E. *et al.* Emergent simplicity in microbial community assembly. *Science* **361**, 469–474 (2018). URL <http://www.sciencemag.org/lookup/doi/10.1126/science.aat1168>.
- [82] Chang, C.-Y. *et al.* Engineering complex communities by directed evolution. *Nature Ecology & Evolution* **5**, 1011–1023 (2021). URL <http://www.nature.com/articles/s41559-021-01457-5>.
- [83] Swenson, W., Wilson, D. S. & Elias, R. Artificial ecosystem selection. *Proceedings of the National Academy of Sciences* **97**, 9110–9114 (2000). URL <http://www.pnas.org/cgi/doi/10.1073/pnas.150237597>.
- [84] Mueller, U. G. *et al.* Artificial Microbiome-Selection to Engineer Microbiomes That Confer Salt-Tolerance to Plants. preprint, *Plant Biology* (2016). URL <http://biorxiv.org/lookup/doi/10.1101/081521>.
- [85] Venturelli, O. S. *et al.* Deciphering microbial interactions in synthetic human gut microbiome communities. *Molecular Systems Biology* **14** (2018). URL <https://onlinelibrary.wiley.com/doi/abs/10.15252/msb.20178157>.

- [86] Cao, H.-T., Gibson, T. E., Bashan, A. & Liu, Y.-Y. Inferring human microbial dynamics from temporal metagenomics data: Pitfalls and lessons. *BioEssays* **39**, 1600188 (2017). URL <http://doi.wiley.com/10.1002/bies.201600188>.
- [87] Maynard, D. S., Miller, Z. R. & Allesina, S. Predicting coexistence in experimental ecological communities. *Nature Ecology & Evolution* **4**, 91–100 (2020). URL <http://www.nature.com/articles/s41559-019-1059-z>.
- [88] Xie, L., Yuan, A. E. & Shou, W. Simulations reveal challenges to artificial community selection and possible strategies for success. *PLOS Biology* **17**, e3000295 (2019). URL <http://dx.plos.org/10.1371/journal.pbio.3000295>.
- [89] Shibasaki, S. & Mitri, S. Controlling evolutionary dynamics to optimize microbial bioremediation. *Evolutionary Applications* **13**, 2460–2471 (2020). URL <https://onlinelibrary.wiley.com/doi/10.1111/eva.13050>.
- [90] Xie, L. & Shou, W. Steering ecological-evolutionary dynamics to improve artificial selection of microbial communities. *Nature Communications* **12**, 6799 (2021). URL <https://www.nature.com/articles/s41467-021-26647-4>.
- [91] Arias-Sánchez, F. I., Vessman, B. & Mitri, S. Artificially selecting microbial communities: If we can breed dogs, why not microbiomes? *PLOS Biology* **17**, e3000356 (2019). URL <https://dx.plos.org/10.1371/journal.pbio.3000356>.
- [92] Cui, W., Marsland, R. & Mehta, P. Effect of Resource Dynamics on Species Packing in Diverse Ecosystems. *Physical Review Letters* **125**, 048101 (2020). URL <https://link.aps.org/doi/10.1103/PhysRevLett.125.048101>.
- [93] Mehta, P., Cui, W., Wang, C.-H. & Marsland, R. Constrained optimization as ecological dynamics with applications to random quadratic programming in high dimensions. *Physical Review E* **99** (2019). URL <https://link.aps.org/doi/10.1103/PhysRevE.99.052111>.

Supplementary Information

Ecological landscapes guide the assembly of optimal microbial communities

Ashish B. George^{1,2,3,*} and Kirill S. Korolev^{1,2,4,*}

¹ *Department of Physics, Boston University, Boston, MA 02215, USA*

² *Biological Design Center, Boston University, Boston, MA 02215, USA*

³ *Carl R. Woese Institute for Genomic Biology and Department of Plant Biology, University of Illinois at Urbana-Champaign, Urbana, IL 61801, USA*

⁴ *Graduate Program in Bioinformatics, Boston University, Boston, MA 02215, USA*

* Correspondence to: ashish.b.george@gmail.com, korolev@bu.edu

December 17, 2021

S1 Ruggedness of community function landscapes

We characterized the structure of community function landscapes using a number of ruggedness measures. We presented the three most useful measures in the main text.

S1.1 Variance unexplained by a linear model

We fit ecological landscapes of community function, $\mathcal{F}(\vec{\sigma})$, by the linear model

$$\hat{\mathcal{F}}^{(1)}(\vec{\sigma}) = a^{(0)} + \sum_{i=1}^S a_i^{(1)} \sigma_i, \quad (\text{S1})$$

where the fit coefficients $a^{(0)}, a_i^{(1)}$ are obtained by least squares regression, which minimizes $(\hat{\mathcal{F}}^{(1)}(\vec{\sigma}) - \mathcal{F}(\vec{\sigma}))^2$.

The fraction of variance unexplained U is given by

$$U = 1 - \frac{\sum_{\vec{\sigma}} (\hat{\mathcal{F}}^{(1)}(\vec{\sigma}) - \bar{\mathcal{F}})^2}{\sum_{\vec{\sigma}} (\mathcal{F}(\vec{\sigma}) - \bar{\mathcal{F}})^2} \quad (\text{S2})$$

where $\bar{\mathcal{F}}$ is mean function; the numerator and denominator are the explained sum of squares and total sum of squares respectively. Note that the variance explained is equal to the coefficient of determination since the mean of the data and fit are equal in least squares regression. U was estimated from a limited number of data points by calculating $\hat{\mathcal{F}}^{(1)}(\vec{\sigma})$ and U using only the sampled data points.

S1.2 Roughness-slope ratio, r/s

The roughness-slope ratio, r/s , compares the fluctuations in community function to the average trend in the function [1, 2]. The roughness r measured the deviation from the best fit linear model in Eq.S13. It is defined as

$$r = \sqrt{\frac{1}{\|\vec{\sigma}\|} \sum_{\vec{\sigma}} (\mathcal{F}(\vec{\sigma}) - \hat{\mathcal{F}}(\vec{\sigma}))^2}, \quad (\text{S3})$$

where $\sum_{\vec{\sigma}} 1$ is the number of points on the landscape. The slope s is given by

$$s = \frac{1}{S} \sum_{i=1}^S |a_i^{(1)}|. \quad (\text{S4})$$

Small r/s values correspond to smooth landscapes—a perfectly linear landscape has $r/s = 0$. Large r/s values correspond to rugged landscapes— $r/s \rightarrow \infty$ for $S \rightarrow \infty$ for a maximally rugged landscape. Since the maximum value of r/s depends on community size, it is used to compare landscapes of the same size only. When analyzing focal species abundance, S is replaced by $S - 1$ since the effective landscape is smaller Eq. S4.

For estimating r/s from a limited number of sampled data points, $\hat{\mathcal{F}}^{(1)}(\vec{\sigma})$ was computed on the sampled points and the sum in Eq. S3 was restricted to the sampled points. For completely flat landscapes, i.e., if community function was constant, we set r/s to zero.

S1.3 Nearest-neighbor correlation and correlation length

We calculated the nearest neighbor correlation Z_{nn} according to the following formula:

$$Z_{nn} = \frac{\frac{1}{\|\vec{\sigma}^{nn}\|} \sum_{\vec{\sigma}, \vec{\sigma}^{nn}} \mathcal{F}(\vec{\sigma}) \mathcal{F}(\vec{\sigma}^{nn}) - \bar{\mathcal{F}}^2}{\sum_{\vec{\sigma}} (\mathcal{F}(\vec{\sigma}) - \bar{\mathcal{F}})^2}. \quad (\text{S5})$$

$\vec{\sigma}^{nn}$ refers to the nearest neighbors of $\vec{\sigma}$ on the landscape, i.e., communities obtained by adding or removing a single species, and $\|\vec{\sigma}^{nn}\|$ is the number of nearest neighbors.

Due to the observed exponential decay of the variance decomposition¹, we can define a landscape correlation length, ξ , given by

$$\xi = \frac{-1}{\ln Z_{nn}}. \quad (\text{S6})$$

ξ specifies the typical number of species one needs to add/remove to reach a new uncorrelated region of the landscape.

S1.4 Fraction of neutral directions

The extrema on the landscape were identified from the relative differences in community function associated with a link between a point and its nearest neighbors:

$$\Delta^B = \frac{\mathcal{F}(\vec{\sigma}^B) - \mathcal{F}(\vec{\sigma}^A)}{\mathcal{F}(\vec{\sigma}^A)} \quad \forall B : |\vec{\sigma}^B - \vec{\sigma}^A| = 1. \quad (\text{S7})$$

¹The nearest neighbor correlation Z_{nn} can also be obtained from the Walsh decomposition [3, 4]

Many links on the ecological landscapes had zero relative difference, either due to a species not being able to invade or the chosen community function being invariant under invasion of the species. The fraction of the links with zero relative difference was recorded as F_{neut} . In simulations, we considered a relative difference of magnitude less than 10^{-4} as zero. In experiments, this threshold would need to be determined from estimates of measurement error or deviation between experimental replicates.

For estimating the fraction of neutral directions and the nearest-neighbor correlation, the landscape was sampled in the same manner. First, we randomly chose $L/2$ points, and then selected an unchosen nearest neighbor for each of the chosen points to make a total of L points. If no unchosen nearest neighbor existed, a random point was chosen instead. F_{neut} and Z_{nn} were calculated on all sampled nearest neighbors.

S1.5 Number of maxima on the landscape

We also computed the number of maxima on the landscape, defined as points with community function greater than or equal to its neighbors (strictly greater than at least one neighbor). We used Eq. S7 with a threshold of 10^{-4} to compare the community function of neighboring points. Most maxima had neutral links associated with it. And so we also counted the number of unique maxima, defined as maxima where all species initially present survived in the final community. The number of unique maxima on the landscape did not correlate significantly with search success.

S1.6 Fitness Distance Correlation, FDC and ranked Fitness Distance Correlation r_{FDC}

The fitness distance correlation, FDC, measures the deviation of the observed landscape from a single-peaked landscape with community function decreasing linearly with distance from the peak [5, 6]. It is given by the Pearson correlation of the community function and hamming distance from the global optimum i.e.,

$$\text{FDC} = \frac{\sum_{\vec{\sigma}} (\mathcal{F}(\vec{\sigma}) - \bar{\mathcal{F}}) (D_{\text{opt}}(\vec{\sigma}) - \bar{D}_{\text{opt}})}{\sqrt{\sum_{\vec{\sigma}} (\mathcal{F}(\vec{\sigma}) - \bar{\mathcal{F}})^2} \sqrt{\sum_{\vec{\sigma}} (D_{\text{opt}}(\vec{\sigma}) - \bar{D}_{\text{opt}})^2}}, \quad (\text{S8})$$

where $D_{\text{opt}}(\vec{\sigma})$ is the hamming distance to the optimum, $\bar{\mathcal{F}}$ is the average community function, and \bar{D}_{opt} is the mean distance to optimum.

We also calculated the Ranked Fitness Distance Correlation r_{FDC} , which computed the correlation of fitness ranks to distance. Both FDC and r_{FDC} vary from -1 to 1 , with $\text{FDC} = -1$ ($r_{\text{FDC}} = -1$) corresponding to a linear (nonlinear but monotonic in distance) landscape with a single peak. Both FDC and r_{FDC} are 0 for an uncorrelated rugged landscape.

We found that these measures tended to be informative only for landscapes of community functions like diversity, which received contributions from all species in the community, and not community functions like the abundance of a focal species.

S1.7 Auto-correlation and correlation length

Instead of performing a gradient-ascent search, one can also explore the community function landscape by taking random steps to nearest neighbors. The random walk auto-correlation, R_{rw} , and the landscape auto-correlation function, R_l are defined with respect to this random exploration of

the landscape [3, 4]. On an statistically isotropic landscape, the random-walk auto-correlation is given by Pearson correlation between points on a random walk trajectory s steps apart i.e.,

$$R_{\text{rw}}(s) = \frac{\langle \mathcal{F}_t \mathcal{F}_{t+s} \rangle - \langle \mathcal{F} \rangle^2}{\langle \mathcal{F}^2 \rangle - \langle \mathcal{F} \rangle^2}, \quad (\text{S9})$$

where \mathcal{F}_t is the community function at step t and $\langle \rangle$ denotes averaging over t over a sufficiently long walk (assuming ergodicity) or averaging over sufficient number of walks with different origins. The landscape autocorrelation is defined as

$$R_{\text{L}}(d) = \frac{\langle \mathcal{F}(\vec{\sigma}_A) \mathcal{F}(\vec{\sigma}_B) \rangle - \langle \mathcal{F} \rangle^2}{\langle \mathcal{F}^2 \rangle - \langle \mathcal{F} \rangle^2} \text{ s.t. } D(\vec{\sigma}_A, \vec{\sigma}_B) = d, \quad (\text{S10})$$

where D measures the Hamming distance between the two points. The two correlation measures are related by

$$R_{\text{rw}}(s) = \sum_d \phi_{sd} R_{\text{L}}(d), \quad (\text{S11})$$

where ϕ_{sd} is the probability that a random walk s steps long is at a distance d away.

For exponentially decaying auto-correlation, we can identify an associated correlation length l defined by the form $R_{\text{rw}}(s) \sim e^{-\frac{s}{l}}$, and estimated as

$$l = \frac{-1}{\ln(R_{\text{rw}}(1))} \quad (\text{S12})$$

S1.8 Species-wise Optimizability, SWO

Species-wise Optimizability SWO quantifies the performance of searching through the landscape by choosing the presence/absence of each species independently [6]. We calculated this by:

1. Choose a starting point A , with presence-absence vector $\vec{\sigma}^A$.
2. For each species i , compare the community function at A with the function obtained by flipping σ_i . Record all i where flipping σ_i increased the community function.
3. Construct the vector $\vec{\sigma}^{A'}$, corresponding to the vector obtained by flipping all recorded σ_i .
4. Repeat steps 1 – 3 for all starting points on the landscape to get sets $\{A\}$ and $\{A'\}$.

Following this, the Species-wise Optimizability SWO is calculated as the ratio of average pairwise distances between the points in the set $\{A'\}$ and points in the set $\{A\}$. We do not estimate SWO from limited data.

S2 Variance unexplained by higher-order models

We fit ecological landscapes of community function $\mathcal{F}(\vec{\sigma})$ incorporating higher-order species interactions using the following class of models:

$$\hat{F}^{(k)}(\vec{\sigma}) = a^{(0)} + \sum_{i=1}^S a_i^{(1)} \sigma_i + \sum_{i=1}^S \sum_{j=1}^{i-1} a_{ij}^{(2)} \sigma_i \sigma_j + \dots \mathcal{O}(a^{(k)}) + \epsilon(\vec{\sigma}), \quad (\text{S13})$$

where the fit coefficients $a^{(0)}, a^{(1)}, \dots$ defined up to order k are obtained by least squares regression minimizing $(\hat{F}^{(k)}(\vec{\sigma}) - \mathcal{F}(\vec{\sigma}))^2$. (Note that these models are linear from the point of view of regression since all the interaction terms are provided explicitly.)

The fraction of variance unexplained by the model of order k , $U^{(k)}$, is given by

$$U^{(k)} = 1 - \frac{\sum_{\vec{\sigma}} (\hat{\mathcal{F}}^{(k)}(\vec{\sigma}) - \bar{\mathcal{F}})^2}{\sum_{\vec{\sigma}} (\mathcal{F}(\vec{\sigma}) - \bar{\mathcal{F}})^2} \quad (\text{S14})$$

where $\bar{\mathcal{F}}$ is mean function; the numerator and denominator are the explained sum of squares and total sum of squares respectively. The variance explained is equal to the coefficient of determination since the mean of the data and fit are equal in least squares regression.

Since inverting matrices becomes computationally expensive for large landscapes, we used an alternative method to calculate the the fraction of variance unexplained. Transforming from presence-absence basis, $\sigma_i \in \{0, 1\}$, to the orthogonal basis $s_i \in \{-1, 1\}$, allows one to use a technique resembling Fourier transforms, called Walsh decomposition [7, 8]. The Walsh/Fourier decomposition of the community function on the transformed landscape ($s_i \in \{-1, 1\}$) is

$$\tilde{\mathcal{F}}(\vec{s}) = \tilde{a}^{(0)} + \sum_{i=1}^S \tilde{a}_i^{(1)} s_i + \sum_{i=1}^S \sum_{j=1}^{i-1} \tilde{a}_{ij}^{(2)} s_i s_j + \dots, \quad (\text{S15})$$

where \tilde{a} are the Fourier components and the expansion continues till order S . Orthogonality allows one to compute each Fourier component without matrix inversion, for e.g.,

$$\tilde{a}^{(0)} = 2^{-S} \sum_{\vec{s}} \mathcal{F}(\vec{s}), \quad (\text{S16})$$

$$\tilde{a}_i^{(1)} = 2^{-S} \sum_{\vec{s}} s_i \mathcal{F}(\vec{s}), \quad (\text{S17})$$

etc. One can then perform a variance decomposition akin to calculating the power spectrum. This variance decomposition gives us

$$2^{-S} (\tilde{\mathcal{F}} - \bar{\mathcal{F}})^2 = \sum_{i=1}^S (\tilde{a}_i^{(1)})^2 + \sum_{i=1}^S \sum_{j=1}^{i-1} (\tilde{a}_{ij}^{(2)})^2 + \dots \mathcal{O}(a^{(S)}) \quad (\text{S18})$$

We can calculate the fraction of the variance explained by a model of order k by truncating the right hand side at order k and normalizing by the total variance i.e.,

$$U^{(k)} = 1 - \frac{1}{\sum_{\vec{\sigma}} (\mathcal{F}(\vec{\sigma}) - \bar{\mathcal{F}})^2} \left[\sum_{i=1}^S (\tilde{a}_i^{(1)})^2 + \sum_{i=1}^S \sum_{j=1}^{i-1} (\tilde{a}_{ij}^{(2)})^2 + \dots \mathcal{O}(a^{(k)}) \right] \quad (\text{S19})$$

We imposed a threshold of 10^{-6} in the fraction of variance unexplained when plotting and fitting data in Fig. 5

S3 Simulations of experimental noise

Two forms of experimental noise was simulated to test robustness of ruggedness estimates in the presence of noise. For simulating additive measurement noise, we modified the community functions

at each point on the landscape as:

$$\mathcal{F}_M(\vec{\sigma}) = \mathcal{F}(\vec{\sigma}) + \overline{\mathcal{F}}\lambda_M\eta(\vec{\sigma}), \quad (\text{S20})$$

where λ_M measures the strength of the noise, η is a normally distributed random variable, and $\overline{\mathcal{F}}$ is the average community function on the landscape. For simulating multiplicative noise, we modified the community function at each point on the landscape as:

$$\mathcal{F}_X(\vec{\sigma}) = \mathcal{F}(\vec{\sigma}) + \mathcal{F}(\vec{\sigma})\lambda_X\eta(\vec{\sigma}), \quad (\text{S21})$$

where λ_X measures the strength of the noise and η is a normally distributed random variable.

S4 Effect of choice of starting point on search efficacy

In the main text, we present the search outcome averaged over all choices of the starting point. We believe this reflects the experimental scenario where information regarding the ideal choice of starting point is limited or even misleading. To evaluate the effect of the starting point on search, we recorded the efficacy of search optimizing Shannon diversity when started from three special choices of the starting community: a community with all species present, a randomly chosen single species present, and a randomly chosen half of the candidate species present. Although intuitively, one expects a higher diversity starting from a community with all species present, the increase in search outcome (over the average search outcome) was very small (0.01, 0.00, and 0.00 for all species, single species, and half species communities respectively, see Fig. S8). Furthermore, the correlation between search outcome and ruggedness remained robust for all three choices of starting communities. Thus, ruggedness is informative of search efficacy from specially chosen starting communities as well.

With intimate knowledge of the system, one can indeed choose special starting points that systematically improve or diminish depending on the community function (at least for simple models). For e.g., consumer-resource models without cross-feeding incorporate only inter-species competition. Therefore, the abundance of a focal species is maximum when it is alone. We are guaranteed to find the optimal community if we start from a community with focal species alone (the optimal community) or one of its nearest-neighbs. It needs to be stressed, however, that this is possible only for specific models and choices of community function—it is unlikely to be relevant for experimental communities.

S5 Supplementary figures

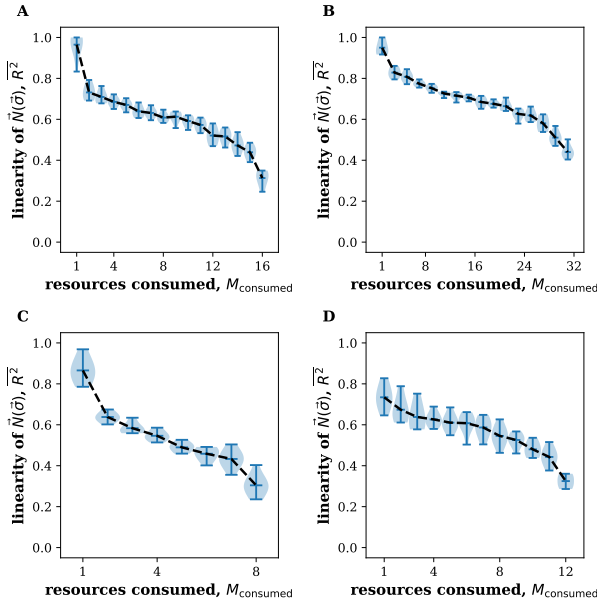


Figure S1: $\vec{N}(\vec{\sigma})$ is linear for specialists and nonlinear for generalists—independent of the number of resources and presence of cross-feeding. The map from species presence to steady-state abundances $\vec{N}(\vec{\sigma})$ becomes more nonlinear with increasing niche overlap across a range of models and parameters. The linearity of the map is quantified by $\overline{R^2}$. Niche overlap increases when species in the pool consume more resources. We plot consumer resource models with $S = 16, M_{tot} = 16$ in (A), $S = 16, M_{tot} = 32$ in (B), and $S = 16, M_{tot} = 8$ in (C); and cross-feeding model with $S = 12, M_{tot} = 12$ in (D). There were 10 replicates for each data point. Simulation parameters are described in Methods.

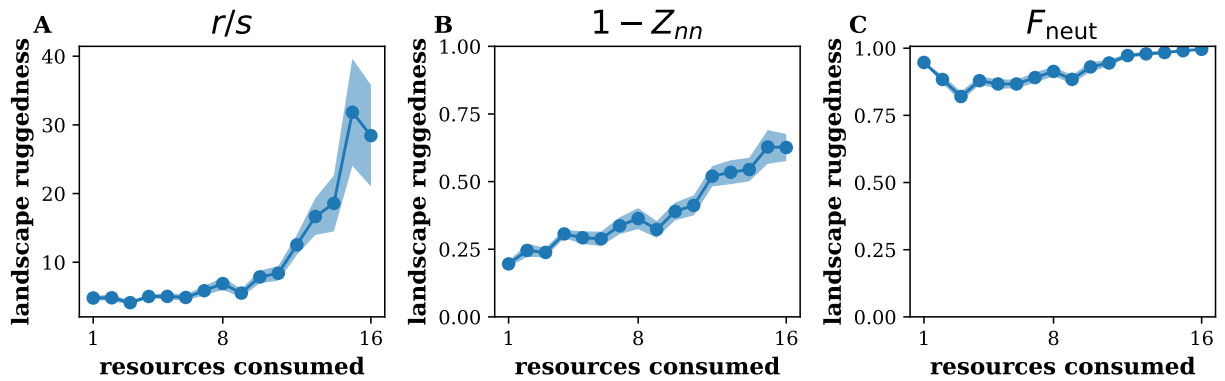


Figure S2: The ruggedness of ecological landscapes of pair productivity. (A,B,C) r/s , $1 - Z_{nn}$, and F_{neut} of the landscape with community function being pair productivity. The fraction of neutral directions F_{neut} was high at low niche overlap, when all of the species occupied separate niches as well, because the species pair responsible for the community function was unaffected by the addition or removal of other species. Simulations were the same as in Fig. 4.

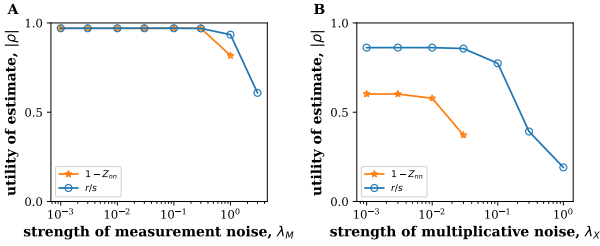


Figure S3: **Estimating search efficacy from noisy data using landscape ruggedness.** Magnitude of the correlation between ruggedness estimated from noisy data and search efficacy remains high even when experimental noise is as large as the community function itself. Two forms of noise were simulated, additive noise in measurement (**A**) and multiplicative noise (**B**). The strength of the noise λ_M and λ_X is measured relative to the community function; therefore a noise strength of one means that the contribution from noise is as large as the community function itself. The community function was the productivity of a pair of species in panel A and diversity in panel B. Noise was simulated as described in SI. Data was obtained from simulations in Fig. 3.

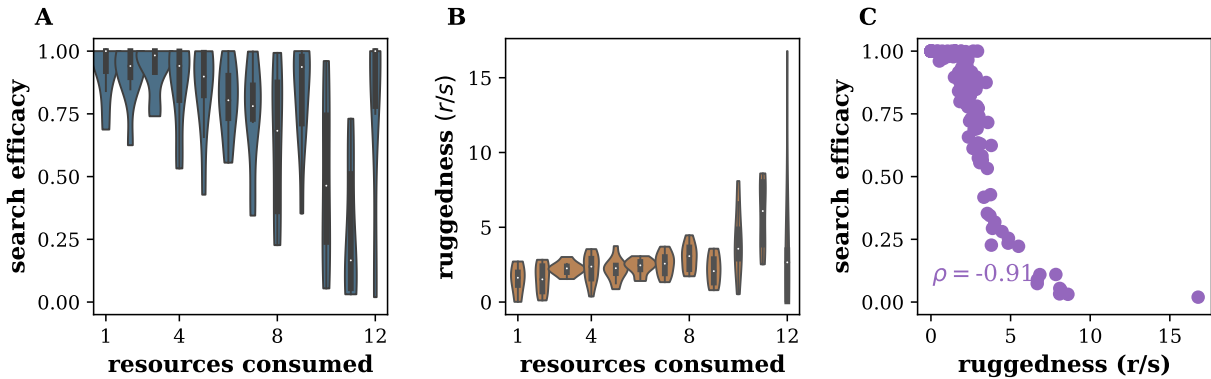


Figure S4: **Niche overlap increases ruggedness and difficulty of search in the presence of cross-feeding.** (A,B) Search outcome and ruggedness of a cross-feeding model where the niche overlap between species was varied by changing the number of resources consumed by each species, mirroring results obtained in model without cross-feeding (Figs. 3, 4). (C) Ruggedness remained informative of search efficacy. Community function was the abundance of a focal species. Parameters are described in Methods.

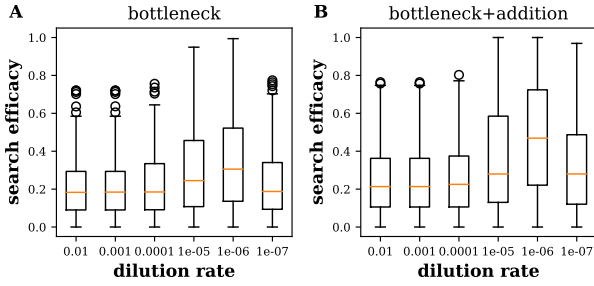


Figure S5: **Performance of dilution-based search protocols is optimal only for a small range of dilution factors.** The dilution-based search protocols, ‘bottleneck’ and ‘addition + bottleneck’, have a high search efficacy only if the bottlenecking step kills a few species but not too many. Therefore, it works best for a narrow range of dilution factors where only order 10 cells survive bottlenecking, before being subject to invasion [10]. Community function was the productivity of a pair of species and simulations were the same as in Fig. 9

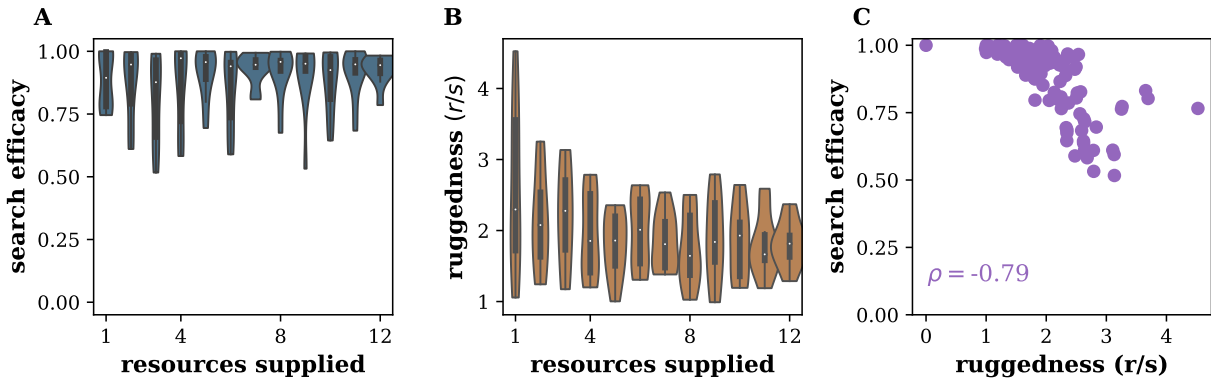


Figure S6: **Landscape ruggedness is informative of search efficacy at different levels of environmental complexity.** (A,B) Search efficacy and ruggedness of a cross-feeding model where the number of resources supplied to the community was varied. (C) Ruggedness remained informative of search efficacy. Community function was the abundance of a focal species. The total amount of resources supplied was held fixed in these simulations with parameters as described in Methods. Simulations where the amount of each resource supplied was held fixed instead gave similar results.

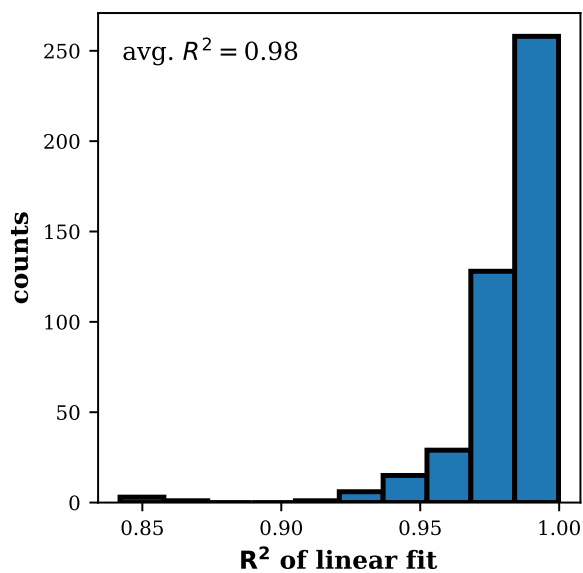


Figure S7: **Rate of metabolic activity is constant over the duration of the experiment.** While the experiment by Langenheder et. al. [9] assayed the cumulative metabolic activity of the microbial communities at different timepoints, used the rate of metabolic activity as the community function. The rate of metabolic activity measured as the slope of a linear fit to the cumulative metabolic activity. The rate was at steady state as evidenced by the high R^2 of linear fit to the data as shown in the figure.

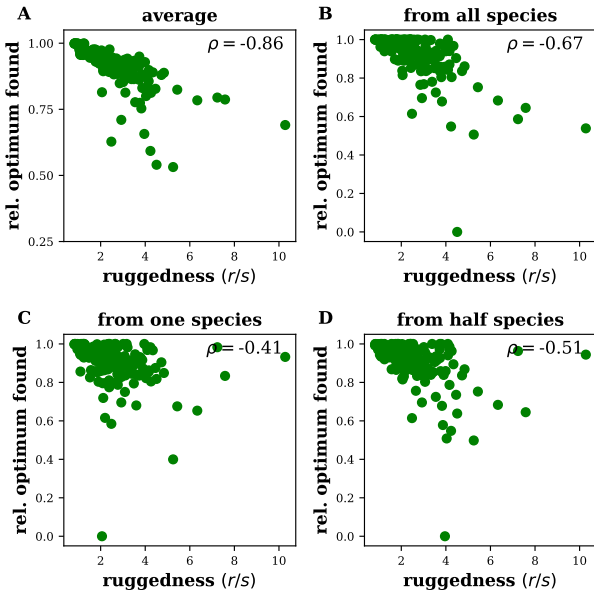


Figure S8: **Ruggedness remains informative of search efficacy even if initial community was fixed.** For Shannon diversity, the ruggedness measure is informative not only about the average search outcome (A), but also about search outcome starting from the community with all species present (B), a randomly chosen species in monoculture (C), and from a randomly chosen community with half the candidate species present (D). Simulation data was the same as in Fig. 4.

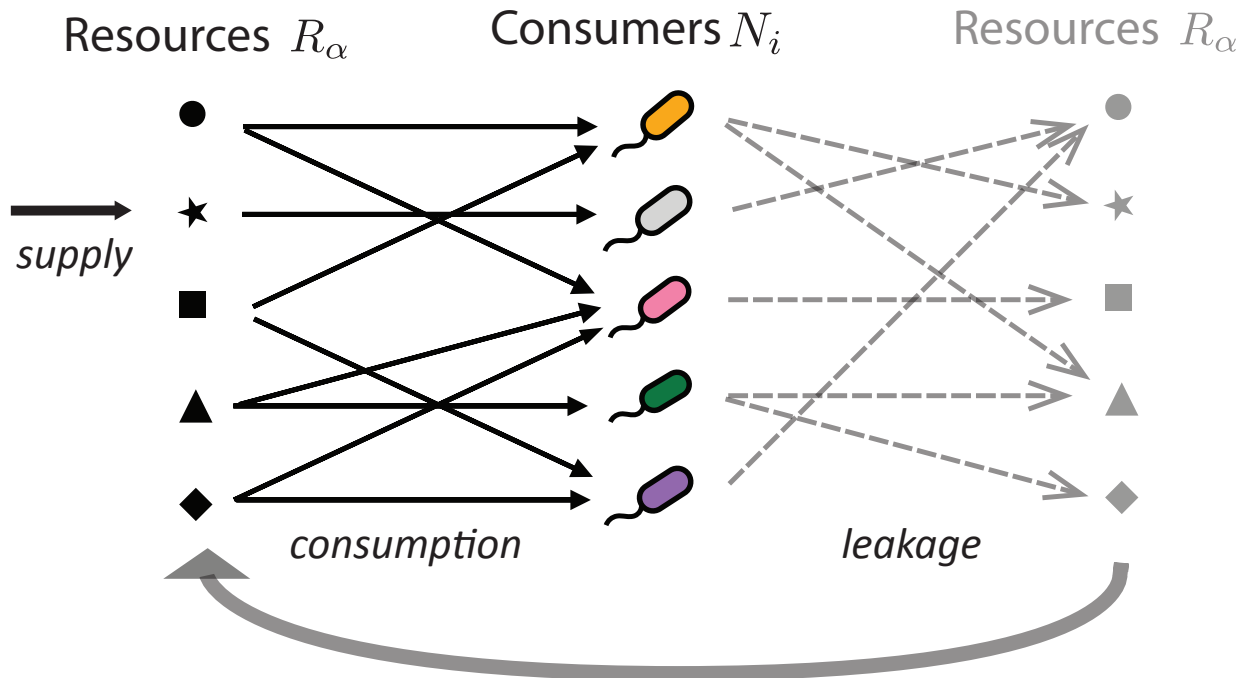


Figure S9: **An illustration of the microbial consumer-resource model.** Species consume resources based on their preferences to grow. Consumption of resources leads to the excretion of consumable byproducts which enables cross-feeding interactions between species.

References

- [1] Aita, T., Iwakura, M. & Husimi, Y. A cross-section of the fitness landscape of dihydrofolate reductase. *Protein Engineering, Design and Selection* **14**, 633–638 (2001). URL <https://academic.oup.com/peds/article-lookup/doi/10.1093/protein/14.9.633>.
- [2] Szendro, I. G., Schenk, M. F., Franke, J., Krug, J. & de Visser, J. A. G. M. Quantitative analyses of empirical fitness landscapes. *Journal of Statistical Mechanics: Theory and Experiment* **2013**, P01005 (2013). URL <http://stacks.iop.org/1742-5468/2013/i=01/a=P01005?key=crossref.80c01de42bec35cf69596036ffc8d086>.
- [3] Weinberger, E. Correlated and uncorrelated fitness landscapes and how to tell the difference. *Biological Cybernetics* **63**, 325–336 (1990). URL <http://link.springer.com/10.1007/BF00202749>.
- [4] Fontana, W. *et al.* RNA folding and combinatorial landscapes. *Physical Review E* **47**, 2083–2099 (1993). URL <https://link.aps.org/doi/10.1103/PhysRevE.47.2083>.
- [5] Jones, T. & Forrest, S. Fitness Distance Correlation as a measure of Problem Difficulty for Genetic Algorithms. In *Proceedings of the Sixth International Conference on Genetic Algorithms: University of Pittsburgh, July 15-19, 1995*, 184–192 (Morgan Kaufmann Publishers Inc., San Francisco, California, 1995). Meeting Name: International Conference on Genetic Algorithms.
- [6] Naudts, B. & Kallel, L. A comparison of predictive measures of problem difficulty in evolutionary algorithms. *IEEE Transactions on Evolutionary Computation* **4**, 1–15 (2000). URL <http://ieeexplore.ieee.org/document/843491/>.
- [7] Stadler, P. F. Landscapes and their correlation functions. *Journal of Mathematical Chemistry* **20**, 1–45 (1996). URL <http://link.springer.com/10.1007/BF01165154>.
- [8] Neher, R. A. & Shraiman, B. I. Statistical genetics and evolution of quantitative traits. *Reviews of Modern Physics* **83**, 1283–1300 (2011). URL <https://link.aps.org/doi/10.1103/RevModPhys.83.1283>.
- [9] Langenheder, S., Bulling, M. T., Solan, M. & Prosser, J. I. Bacterial Biodiversity-Ecosystem Functioning Relations Are Modified by Environmental Complexity. *PLoS ONE* **5**, e10834 (2010). URL <https://dx.plos.org/10.1371/journal.pone.0010834>.
- [10] Chang, C.-Y. *et al.* Engineering complex communities by directed evolution. *Nature Ecology & Evolution* **5**, 1011–1023 (2021). URL <http://www.nature.com/articles/s41559-021-01457-5>.